“Franken-CARD9”: chimeric proteins for high-resolution studies of activating mutations in CARD10, CARD11 and CARD14

Jens Staal[1,2,3,#], Yasmine Driege[1,2], Femke Van Gaever[1,2], Jill Steels[1,2], Rudi Beyaert[1,2]

[1] Unit of Molecular Signal Transduction in Inflammation, VIB-UGent Center for Inflammation Research, Ghent, Belgium
[2] Department of Biomedical Molecular Biology, Ghent University, Ghent, Belgium
[3] Department of Biochemistry and Microbiology, Ghent University, Ghent, Belgium

[#] Author for correspondence: Jens Staal < jens.staal@irc.vib-ugent.be >

Keywords: protein engineering, signal transduction, cancer, glaucoma, inflammation, natural variation, UK biobank, reverse genetics

Abstract

CARD9, -10, -11 and -14 all belong to the CARD-coiled coil (CC) protein family and originated from a single common ancestral protein early in vertebrate evolution. All four proteins form CARD-CC/BCL10/MALT1 (CBM) complexes leading to NF-κB activation after upstream phosphorylation by various protein kinase C (PKC) isoforms. CBM complex signaling is critical for innate and adaptive immunity, but aberrant activation can cause autoimmune or autoinflammatory diseases, or be oncogenic. CARD9 is the only family member that has retained the original domain organization. The other family members have been fused to a C-terminal ZO-1/Dlg5-like MAGUK domain, forming the CARMA sub-family. CARD9 shows a superior auto-inhibition with very low spontaneous activity when overexpressed in HEK293T cells. In contrast, the poor auto-inhibition of other CARD-CC family proteins, especially CARD10 (CARMA3) and CARD14 (CARMA2), is hampering characterization of upstream activators or activating mutations in overexpression studies. We grafted different domains from CARD10, -11 and 14 on CARD9 to generate chimeric "Franken-CARD9" backbones for functional characterization of activating mutants using NF-κB reporter gene activation in HEK293T cells as readout. This revealed that most of the poor auto-inhibition of CARD10 and CARD14 can be mapped to the CARD10 LATCH and CARD14 CARD domains, respectively. CARD11 (CARMA1) activity was not further reduced by grafting on Franken-CARD9 backbones. The Franken-CARD9 approach was subsequently validated by using several known disease-associated mutations in CARD10 and CARD14, and additional screening allowed us to identify several novel activating natural variants in human CARD9 and CARD10. Using Genebass as a resource of exome-based disease association statistics, we found that activated alleles of CARD9 correlate with irritable bowel syndrome, constipation, arthritis, fibromyalgia, insomnia, anxiety and depression, which can occur as comorbidities.

Introduction

The CARD-CC/BCL10/MALT1-like paracaspase (CBM) complexes are critical for signaling leading to pro-inflammatory gene expression. Dysregulation of the CBM complexes has been associated to many immune-related diseases and cancer [1]. The CBM complexes are ancient and can be found as far back as Cnidaria [2]–[4]. In vertebrates, there are four distinct CBM complexes (CBM-9, CBM-1, CBM-2 and CBM-3) defined by the different CARD-CC protein family members: CARD9, CARD11 (CARMA1), CARD14 (CARMA2) and CARD10 (CARMA3), respectively [5]–[7]. This expansion of the monophyletic CARD-CC family coincides with an expansion of many functionally associated immune-related genes early in vertebrate evolution, most likely as a consequence of genome duplication [3], [8], [9]. CARD9 has retained the domain structure of the ancestral CARD-CC protein found in invertebrates, a sister group with the last common ancestor found in tunicates. The other paralogs (CARD10, -11 and -14) have all obtained a C terminal fusion with a ZO-1/Dlg5-like MAGUK domain (Fig. 1a) [2], [10], [11], forming the CARMA sub-family. A common theme between the four jawed vertebrate CARD-CC proteins is that they all get activated by protein kinase C (PKC) [11], and will subsequently form filamentous polymeric filaments by aggregation via their CC domain [4], [12]–[15]. These CARD-CC filaments will bind

the signaling proteins BCL10 and MALT1 via the CARD domain, which subsequently will signal towards NF-κB activation and activation of the paracaspase MALT1 protease activity [16]–[21]. The recruitment of the BCL10/MALT1 complex to the CARD-CC protein is a critical signaling event and BCL10 fusion to CARD11 results in a constitutively active signaling complex [22]. The normal sequence of events is however most likely phosphorylation leading to CC domain aggregation and subsequent BCL10/MALT1 recruitment to the exposed CARD domain [15], [23]–[26]. Despite their similarities, the four CARD-CC proteins are distinguished especially by their expression profile, where CARD9 and CARD11 are primarily expressed in innate and adaptive immune cells, respectively, and CARD10 and CARD14 primarily in different non-hematopoietic cells. The cell type specific expression differences also influence the phenotypes of mutants in the different CARD-CC family members [27]. Loss of function mutations in CARD11 cause severe combined immunodeficiency (SCID) due to a defective adaptive immunity [28]. Weaker hypomorphic mutations of CARD11, in contrast, cause hyper-IgE syndrome (HIES) with atopic dermatitis, a phenotype also seen when downstream MALT1 is lost [29]–[32]. Loss of function mutations in CARD9 cause a defective innate immune response to especially fungal infections [33], [34], and the combined loss of CARD9 and MyD88 cause a severe disruption of innate immunity since two central adaptor proteins for different innate immune receptor signaling pathways are lost [35]. The only potential "activating" known disease-associated germ line CARD9 mutant would be $CARD9^{S12N}$ [36], but this mutation is recessive and only enhances expression of some RelB-dependent cytokines after upstream receptor stimulation. The enhanced RelB-dependent gene expression is supposedly due to reduced MALT1-mediated RelB cleavage, which means that the S12N mutation is not an activated CARD9 mutation. This mutation is thus more in line with other CARD11 mutations that show a complex phenotype that indicates features of both gain- and loss-of-function [37]. There are no strong reports on phenotypes from loss of function mutations in CARD10 or CARD14, but it has been suggested that loss of CARD14 could sensitize to the development of atopic dermatitis [38]. Mice deficient for *Card10* show neurodevelopmental defects, a phenotype shared with *Bcl10* deficient mice [39], [40]. Human germ line and somatic mutations in CARD10 have been suggested to be associated to immunodeficiency, autoimmunity, cancer, cognitive defects and primary open-angle glaucoma (POAG), but it is not established whether the mutations are activating or inactivating [41]–[43]. High expression of CARD10 or CARD14 have both been associated to increased cancer cell survival [44], [45]. Up until now have germ line activating mutations in CARD-CC proteins only been found in CARD11, which result in B cell lymphomas and *B cell expansion with NF-κB and T cell anergy* (BENTA) [46], [47], as well as CARD14, which results in psoriasis or *Pityriasis rubra pilaris* (PRP) [48]. For both CARD14 and CARD10, the functional characterization of activating mutations is often hampered by the very high basal activity during transient overexpression studies, which leads to no or poor enhancement of the relative NF-κB activation from the activating mutations compared to wild-type (Fig. 1b) [11], [19]. We generated so-called chimeric proteins in order to exploit the superior auto-inhibition properties of CARD9 to functionally characterize mutations from the other CARD-CC family members. The concept of a chimera originates from a mythological monster created by parts of different animals [49], [50]. In a very similar way, our chimeric CARD-CC proteins are artificially made by transplantation and replacement of functionally conserved parts to generate a novel but fully functional protein. The functionally conserved paralog sequences that we use have diverged during at least 500 million years of independent evolution, since the split between CARD9 and

the CARMA proteins occurred before the last common ancestor of hagfish and jawed vertebrates [11], [51].

Results

Sequence alignment can identify activating mutations transferable from CARD11 to CARD9

Earlier structural comparisons between CARD9 and CARD11 have focused on the N terminal parts of the two proteins, and did not include the complete CC domain. It was demonstrated in those comparisons that several activating oncogenic CARD11 mutations in the CARD and LATCH domains are translatable to CARD9 [15], for example the CARD9^{G111S} mutation, which corresponds to the CARD11^{G123S} mutation (rs387907352) associated with BENTA [52]. We have previously also utilized the strategy of transfering a CARD11 oncogenic mutation located further downstream in the CC domain (L232LI) [53], [54], to CARD9^{L213LI} for functional characterization of an inactivating mutant [33]. The same mutation has also been transfered to CARD10^{L237LI} and CARD14^{L229LI}, but due to the high basal activation of the wild-type variants of those proteins, the effect of the mutations was only apparent at very low expression levels [11]. The CARD9 T231 site is highly interesting since it is critical for activation downstream of several different PKC isoforms [11], [55]. This residue aligns nicely with CARD11 S250 (Fig. 1b), and CARD11^{S250P} is a known oncogenic activating mutation [46]. Interestingly, while the CARD9^{L213LI} gives a strong activation, this is clearly dwarfed by the exceptional activation that can be seen from the CARD9^{T231P} mutation (Fig. 1b), demonstrating that this mutation is superior for functional characterization of activated CARD9. Consistent with previous observations [11], [15], [33], we see that inactive CARD9 shows strongly reduced protein expression (Fig. 1b), which may be part of the auto-inhibition mechanism.
Since, to our knowledge, no germ-line activating mutations have been found or described in CARD9 [27], we investigated natural potentially activating substitutions from human sequence data in Uniprot [56]. One of the most striking candidate germ line activating CARD9 mutations is a natural CARD9 variant causing the very rare CARD9^{G111E} mutation (rs371695061), corresponding to the BENTA-associated CARD11^{G123D} mutation (rs571517554) — which is more severe than the previously mentioned CARD11^{G123S} BENTA mutation [47]. At this moment, there is no disease phenotype associated with this activated variant of CARD9. However, the top disease associations to CARD9^{G111E} (9-136371136-C-T) in Genebass [57] seem to be related to: constipation, IBS, fibromyalgia, arthritis, pain, insomnia anxiety and depressive behaviors. Interestingly, all of these disease conditions are well-known comorbidities [58]–[60], and a risk locus for IBS with constipation (IBS-C) in women has been mapped close to CARD9 on chromosome 9 [61]. Also several other potentially activating mutations in addition to CARD9^{G111E} can be found in the human natural variation of CARD9, for example: L85F (rs1239721232; L85Y shown to be activating [15]), Y86C (rs1049019466; Y86F shown to be activating [15]), R101H (rs988002931; R101Q shown to be activating [15]) and V102I (rs1490862744). Testing these potentially activating natural variations revealed that only CARD9^{G111E} caused strong spontaneous activation of CARD9 (Fig. 1c), with the other mutants being less active or approximately as active as wild-type CARD9. The CARD9^{G111E} is approximately as active as the

very strong artificial CARD9^{T231P} mutation (Fig. 1b,c), indicating that it probably is close to the highest level of spontaneous activity that can be generated. One problem with CARD9^{G111E} is that it is an extremely rare mutation – with a single case in the Genebass database (out of 394841 individuals). The same mutation can not be found in GnomAD 2.1 [62], but G111R (9-139265589-C-T (GRCh37), rs769183409) has 3 individuals out of almost 250000 with an age range of 40-50 years old. This indicates that carriers of substitutions at this site are viable, but there is no health data publicly available for these individuals. Strucural predictions at the G111 site indicate that any substitution at this site should be activating [15]. To test this, we generated a CARD9 mutant (G111A) with a structural disruption as small as possible at this site. Interestingly, this substitution was almost as active as the G111E substitution (Fig. 1d), confirming the structural prediction that any substitution at G111 should be activating. Different natural CARD9-activating mutations associated to the same sequelae would give more confidence to the predicted disease associations in Genebass, since it would exclude linkage to other disease-causing mutations. By listing missense mutations associated to one disease condition (fibromyalgia) associated to CARD9^{G111E} in Genebass, several other candidate natural mutations (K165E (rs781419489), S172N (rs201802044), E523Q (rs144943839) and *537Qext59* (rs1405807688)) can be identified which also have associations to psychological and gastrointestinal problems. By using a disease phenotype or alternative substitutions at the same site as an activating mutation, we can also identify additional potentially activating substitutions, such as K165del (9-136370972-CCTT-C) and E523K (rs144943839). Testing these mutations revealed that all of the fibromyalgia-associated variants and alternative variants in the same residues are activated, showing that fibromyalgia association is a very good predictor of activated CARD9 variants (Fig. 1d). The L423V (9-136367639-G-C) mutation was not identified by association to fibromyalgia, but rather due to other comorbidities (constipation, pain) overlapping with the top disease associations for the K165E and *537Qext59* variants. The lack of activation in this variant highlights that fibromyalgia remains the best predictor of activated CARD9 variants for now. Interestingly, the level of activation in our overexpression system seems to be correlating with the increased frequency of fibromyalgia: Weak activating CARD9 mutations (S172N, E523Q) show a 3-fold higher frequency (3/372) of fibromyalgia compared to the total population (1176/394841). Intermediate mutations (K165E, K165del) a 6-fold (1/56) and strong mutations (G111E, *537Qext59*) show a 48-fold increased frequency (2/14) of fibromyalgia compared to the total population. The low number of cases will however make those estimates quite uncertain. A full auto-activation survey of the CARD9 natural variations in humans and targeted investigations of CARD9 in patients with associated disease phenotypes for novel rare variants may be able to pick up even more disease-associated alleles in the future. It might also be possible to run itterative cycles of reverse genetics by *in vitro* testing of candidate mutations associated to the same diseases, and the new activated mutations could then form a new training set for another cycle of disease associations.

The CARD9 C terminal sequence downstream of the CC domain is inhibitory in CARD9, -10, -11 and -14

Transfering activating mutations from CARD11 to CARD9 is generally far easier than to transfer activating mutations from for example CARD14 to CARD9, since CARD11 has diverged far less from CARD9 and typically aligns better [2], [11]. In order to solve this issue, we investigated whether we could create hybrid proteins with the advantages of CARD9, such as the strong

auto-inhibition and high fold-induction when activated, with sequence segments grafted from the other CARD-CC family members to enable direct transfer of known mutations into this "Franken-CARD9" (or "pseudo-CARD9") backbone. We have previously observed that deletion of the sequence downstream of the CC domain in CARD9, -10, -11 and -14 causes a spontaneously active protein [2], [33], indicating that the C-terminal part of CARD9 acts as the "inhibitory domain" (ID) analogously to the linker sequence downstream of the CC domain in CARD11 [25]. Also, in our screening for activated natural variants in CARD9, we identified two variants (E523K, *537Qext59*) that disrupt the autoinhibitory activity of this C-terminal sequence (Fig. 1d). With that in mind, we fused the CARD9 C-terminal sequence to the CARD-LATCH-CC part of CARD10, CARD11 and CARD14. As comparison, we also generated proteins with a CARD9-like domain structure (creating a "pseudo-CARD9" with no sequences derived from CARD9) by deleting the C terminal MAGUK domain in the three CARMA proteins. The linker/ID sequences are not highly conserved, but looking at the Alphafold [63] structures it seems like all the flexible linkers downstream of the CC domain either wrap around or go in between the two long alpha helices that constitute the CC domain, which could mean that they all fulfill the same role for auto-inhibition (Fig. 1a). Interestingly, the CARD9 C-terminal sequence was either equally good or better than the native sequence downstream of the CC domain to provide some measure of auto-inhibition for all the CARD-CC variants (Fig. 2a). This is in contrast to previously generated hybrid proteins, where the CARD14 ID/linker was unable to maintain CARD11 auto-inhibition [25].

The CARD9 CARD domain offers additional auto-inhibition

In a recent study focusing on the structure of the CARD, LATCH and early part of the CC domains, some residues were identified in the CARD9 CARD domain, compared to the CARD11 CARD domain, which contributed to an enhanced auto-inhibition of CARD9 [15]. We could see a similar effect from the C terminal deletion constructs, where the CARD9 N terminal construct showed less activity than the other corresponding constructs (Fig. 1c). Because of this, we replaced the CARD domain with the CARD9 CARD domain in our CARD-LATCH-CC clones from CARD10, CARD11 and CARD14 with the C terminal CARD9 sequence (Fig 2a). The very strong spontaneous activation seen in the CARD14 clones (Fig 1c) was eliminated in the CARD replacements (Fig. 2b), indicating that a major reason for the poor autoinhibition of CARD14 lies in the CARD domain.

CARD9 LATCH replacements influence auto-inhibition

Despite being a small sequence segment that is poorly conserved, especially in CARD14 [15], is the LATCH (a.k.a α-linker) region between the CARD and CC domains highly interesting since many activating mutations in CARD11 and CARD14 map to this region. Due to this, we initially also swapped the CARD-LATCH domains (Fig. 2b). While the CARD domain clearly influenced the spontaneous activity of CARD14, CARD10 spontaneous activity was specifically affected by the LATCH domain. To ensure that this was a domain-intrinsic effect and not a specific interaction with the CC domain, we also did the opposite domain swapping and swapped either the CARD or CARD-LATCH domain of CARD9 with the corresponding sequences from CARD10, CARD11 or CARD14 (Fig. 2c). This inverted effect verified that the small LATCH domain has a significant

influence on the basal activity of the protein, which is corresponding to the location of many known activating mutations. It also verified that a major contributor to the poor autoinhibition in CARD14 is the CARD domain. That the effect was visible independently of which CC domain was used indicates that the effect is not entirely due to specific inter-domain interactions as is proposed by the standard model of CARD-CC activation [54]. Inter-domain interactions do however have some effect since we see synergistic effects from CARD and LATCH domains in spontaneous background activity (Fig. 2b,c). To study the LATCH domains in isolation, we also replaced only the LATCH domains (Fig. 2d), which strongly highlighted and verified the role of the CARD10 LATCH domain in the poor auto-inhibition. Based on sequence comparisons, it is very surprising that CARD10 and CARD11 LATCH domains cause less auto-inhibition than the CARD14 LATCH, which is a poorly conserved sequence (Fig. 2d). The CARD10 LATCH only has 7 significant substitutions in 3 segments, compared to the CARD9 LATCH (Fig. 2d,e). We found that two of the three substitution segments between the CARD9 and CARD10 LATCH domains contribute additively to the autoinhibition (Fig. 2e), which means that the complete CARD9 LATCH is needed for lower background signal in Franken-CARD10 constructs. In order to validate that the mapped domains for auto-inhibition also are relevant in the original backbone, we generated a CARD10 clone with the CARD-LATCH transplanted from CARD9 (CARD10-9CL) and a CARD14 clone with the CARD transplanted from CARD9 (CARD14-9C). While the LATCH clearly is contributing to the auto-inhibition in CARD14 (Fig. 2b,c), it also is a site where many psoriasis-associated mutations are located (Table 4). Compared to wild-type CARD10, CARD10-9CL was clearly less auto-activated (Fig. 2f), which means that this could be a good backbone for mutant testing since most disease-associated mutations in CARD10 are located in the CC domain or further downstream [42]. CARD14 with the CARD domain replaced with CARD9 CARD did however not show any notable reduction of auto-activation compared to wild-type CARD14 (Fig. 2f), indicating that more domains are important in this regulation.

Using the chimeric Franken-CARD9 constructs to analyze activating mutations

As two case studies, we use the B cell lymphoma CARD11 CC mutation L232LI [53] and the pustular psoriasis CARD14 CC mutation E138A [64]. For the CARD11 L232LI mutation, we could see an interesting inter-domain interaction effect: while the corresponding CARD9^{L213LI} mutation was activating, the CARD9 with only CARD11 CC was not activated by the L232LI mutation (Fig. 3a). Activation by the CARD11^{L232LI} mutation required CARD11 LATCH. Taken together, this indicates that activation by the L/LI substitution requires a matching LATCH-CC interaction. In contrast, the activation by the CARD14^{E138A} mutation was domain-intrinsic and the strongest relative fold-induction was seen in CARD9 with only the CARD14 CC domain transplanted (Fig. 3b). While the CARD9-14LCC (CARD14 LATCH-CC) showed less than 2-fold activation from the E138A mutation, the same mutation in the CARD9-14CC backbone caused several 100-fold activation, demonstrating the importance of low background activity to reliably detect the effect of activating mutations by transient overexpression.
Since the CARD14 LATCH domain and the CC domains from CARD10 and CARD14 caused relatively mild auto-activation after transplantation to CARD9 (Fig. 2a,c), we investigated published mutations in these domains as a proof-of-concept of the Franken-CARD9 strategy. For CARD14 LATCH we could not see any activation from LATCH domain psoriasis-associated

mutations, except for L124P (Fig. 4a). This surprising result indicates that the activation from CARD14 LATCH mutations requires specific interactions with other CARD14 domains, probably the end of CARD and beginning of CC [15]. It does challenge the model that activating mutations are disrupting inter-domain interactions, however, since the CARD14 LATCH Franken-CARD9 chimera is auto-inhibited. We had already seen that CARD14 CC was a good candidate Franken-CARD9 construct (Fig. 3b), and this allowed us to investigate several psoriasis and PRP-associated mutations in the CARD14 CC domain to confirm that this strategy is generally applicable. All the mutations were strongly activating in the CARD9-14CC construct (Fig. 4b). The E138 allelic series showed that the PRP mutation E138K was a stronger activator than the two psoriasis-associated mutations E138A and E138del, in line with the suggested correlation between mutation strength and disease phenotype [48].

At this moment, no association has been made between a disease condition and activating mutations in CARD10 [27]. However, several germline mutations in the CARD10 CC domain have been found associated to diseases, such as primary open angle glaucoma (POAG), or as a single case of autoimmunity / immunodeficiency (R420C) [41], [42]. There are also somatic CARD10 mutations described in cancers [43], and since CARD10 overexpression is associated to some cancers [65], those mutations are also good candidates for activating CARD10 mutations. Surprisingly, all mutations except one (R212H; ClinVar: VCV000224912.1; dbSNP: rs1057519378) were as active as the wild-type CARD9-10CC construct (Fig. 4c). Interestingly, CARD10 R212 aligns with R207 in CARD11 — and the CARD11 R207H mutation has been picked up in genetic B cell lymphoma screenings [66], [67] — which supports that this mutation is likely to be activating. In comparison to the extremely rare activated CARD9^{G111E} allele, CARD10^{R212H} is far more common, with 25 cases out of 394841 being reported in the Genebass database. The lack of activation from the other CARD10 mutations tested could either be a limitation of the Franken-CARD9 construct due to inter-domain dependencies similar to the CARD11 L/LI mutation (Fig. 3a), or biologically true since there is no prior evidence that these disease-associated mutations are activating. To investigate the first possibility, we re-cloned the mutations into the CARD10-9CL Franken-CARD10 construct, which shows much lower auto-activation compared to wild-type CARD10 (Fig. 2f). In line with the CARD9-10CC constructs, R212H was the only CARD10 mutation that activates also in the CARD10-9CL backbone (Fig. 4d). In contrast to the psoriasis-associated CARD14 mutations in the CARD9-14L and CARD9-14CC backbone, the POAG-associated CARD10 mutation R212H only results in a very moderate relative activation. In this initial screening we have only evaluated CARD10 variants that have been associated to disease in literature. Since published disease associations seem to be a poor predictor of activating CARD10 variants, a broader screening was done. The R212 position has multiple natural variations (R212C (rs760871700), R212L (rs1057519378)), which potentially could represent additional activating variant alleles. Sorting for candidate activating mutations by disease in Genebass did not pick up candidates with an as uniform pattern of comorbidities in CARD10 as with activated CARD9, but some candidates (R142Q (rs199764326 ; cardiovascular), E145K (rs769979914), R153P (rs1187928736; kidney), and R364Q (rs199557110 ; allergic rhinitis)) were considered good starting points for seeding a more accurate prediction model for activating mutations based on disease associations. We included the E145K variant based on its similarity to the activating psoriasis-associated substitutions E138K and E142K in CARD14 (Fig. 4b). The screening verified two new activated variants (R153P, E145K), and surprisingly one inactivated variant (R142Q) (Fig. 4e). Based on disease associations in common between the

verified activated variants available in Genebass (R153P, R212H), “acute nephritic syndrome” is the most promising disease association as a predictor of new candidate activated CARD10 variants. Using this association, we tested E390A (22-37507851-T-G) and R364W (rs184229951), which were not activating (Fig. 4e). This means that disease associations so far has failed to predict activating CARD10 variants. The surprising finding of an inactivating (R142Q) CARD10 mutation is also very interesting, since no human disease has been associated with CARD10 loss-of-function. All other CARD-CC members have reported diseases from loss-of-function in humans: CARD11 loss causes severe combined immunodeficiency (SCID), CARD9 loss causes impaired innate immunity against fungi and CARD14 loss has been suggested to cause atopic dermatitis. Screening for additonal inactivating CARD10 natural variants using the potential link to cardiovascular disease and other related disease phenotypes (like “platelet distribution width”) could thus also be informative.

Discussion

Regulation of CBM complex signaling is critical since dysregulation can cause inflammatory diseases [64] and cancer [53], [68], [69]. Functional characterization of mutations in some of the CARD-CC proteins can however be problematic due to their high base line activity [11], [19], [64]. While highly artificial, we have demonstrated that utilization of CARD9 as a backbone enables us to study mutants from the other CARD-CC family members by swapping the corresponding region between both the proteins to generate hybrid chimeric CARD-CC proteins, even when the sequences are not conserved. The chimeric proteins all fully activate down-stream signaling, with some protein domain transplantations resulting in reduced or inefficient auto-inhibition. This indicates that critical intramolecular interactions that keep the protein in an inactive state represent a significant divergence between the CARD-CC paralogs. A striking unique advantage here with the CARD9 backbone seems to be the inhibitory capacity of the C terminal sequence, which is able to auto-inhibit all the other paralogs (Fig. 1c). This is in contrast to previous studies, where it was shown that the transplanted CARD14 ID/linker sequence is unable to inhibit CARD11 [25]. With our use of the Franken-CARD9 backbones, it seems like some activating mutations act internally on the domain where they are located, which is in contrast to previously reported models where mutations were proposed to disrupt intra-molecular but inter-domain interactions between CARD, LATCH and CC or between CC and ID [15], [23], [54]. Utilization of functionally conserved but sequence-diverged protein domains is a powerful complementary approach to specific site-directed mutagenesis in order to understand the mechanisms and structural constraints for protein function [2], [70], [71]. For example, there is a high representation of psoriasis-associated CARD14 mutations in the poorly conserved LATCH domain (Fig. 3b, 4a). Franken-CARD9 constructs to study these CARD14 LATCH mutations still need further optimization since only one mutation (L124P) was activating. Identification of the required surrounding sequence for a functional Franken-CARD9 CARD14 LATCH psoriasis mutation reporter will also give further structural insight in how gain-of-function mutations require specific interactions with those surrounding sequences. As can be seen with many constructs, the CARD9 backbone results in dramatic fold inductions, while the same mutations in the native protein give much weaker effects due to a higher background signal. A major reason for this is the superior auto-inhibition of the CARD9 C-terminal sequence that we have

exploited here, but also the fact that this sequence has been shown to contribute to downstream signaling in activated CARD9 [72], [73], which could explain why the CARD9$^{\Delta C}$ construct is much less active than the CARD9^{G111E}, CARD9^{L213LI} and CARD9^{T231P} constructs. The chimeric CARD-CC proteins could also be useful to investigate CARD-CC isoform-specific signaling downstream of the CBM complexes by studying the contribution of each domain in isolation. The sequence-swapped Franken-CARD9 construct should also be ideal for mapping of interacting proteins that specifically bind one CARD-CC isoform. An advantage with these constructs is that they will look and act approximately the same except for the sequence that has been swapped, so there should be fewer artifacts from deletion-induced spontaneous activation or other structural changes. Up until now, only naturally occurring activating germ line mutations have been described in CARD11 (causing B cell lymphoma and BENTA) and CARD14 (causing psoriasis and PRP) within the CARD-CC family [27]. Activating mutations are typically dominant, and will thus usually be less frequent than recessive loss-of-function mutations if detrimental.

By sequence comparisons with CARD11 and screenings of candidate activating natural variants, we could for the first time establish that there are activating CARD9 mutations in the human germline, and public disease association data could be used to mine for more candidate activating variants with similar disease associations. The identification of activating germ-line mutations in CARD9 could be done rapidly by a simple overexpression assay thanks to its intrinsically good auto-inhibition (Fig. 1c). Using our novel Franken-CARD9 framework, we could also do a similar simple overexpression-based screening to establish that the POAG-associated CARD10 mutant R212H is activating (Fig. 4c,d), demonstrating that there are germ line-inherited activating mutations also in CARD10. To our surprise, the majority of the POAG-associated CARD10 mutations evaluated in our models did not show signs of gain-of-function — or loss-of-function. Since there are multiple independent mutations in CARD10 that are associated to POAG, it is very likely that those mutations are truly causative of the disease. It is however possible that the activation effect of the CARD10^{R212H} mutation is unrelated to the POAG disease phenotype. Due to the low success rate in finding activating CARD10 mutants by screening published disease-associated mutations, future screening for activating natural variants in CARD10 should probably rather be focusing on other predictions, like the AlphaFold structure [15], [63] or similarity to other activating mutations. This was also how we identified the activating CARD10^{E145K} variant. Also disease associations that are overlapping with phenotypes displayed by carriers of already known activating variants in CARD10 could be very informative, as demonstrated by our identification of the activating CARD10^{R153P} variant based on the disease associations of CARD10^{R212H}.

The relatively mild phenotype (POAG) officially associated to the activated CARD10^{R212H} is quite surprising considering the broad expression profile of CARD10, and the quite severe diseases that are associated to genetic activation of CARD11 in lymphocytes and CARD14 in keratinocytes. It is possible that the phenotypic effect of CARD10 activating mutations is blunted thanks to the MALT1 protease-mediated negative feedback regulation through CARD10 cleavage [74]. There are natural known variations in the CARD10 cleavage site R587 (R587Q or R587P ; rs746691823 and R597W ; rs1039088798), reported in Genebass, which seem to be associated to cancer and cardiovascular disease [57]. This cleavage site (R587) is however not present in our CARD9-10CC constructs, where residues 134-450 of CARD10 are transplanted to CARD9 (Table 1). We also did not see any cleavage of the CARD9-10CC constructs (Fig. 4c).

The activating mutations in CARD9 and CARD10 were only picked up as a heterozygote and very rare, which indicates that they are (co-)dominant activating mutations. The dominant nature of the gain-of-function activating mutations allowed us to identify potential novel disease associations with the six activated CARD9 variants and three activated CARD10 variants that we identified in our screening. In contrast, rare recessive loss-of-function mutations are often only causing disease in populations with high levels of endogamy [75], which would have been difficult to pick up in Genebass due to limited ethnic diversity in the UK Biobank dataset [57]. Hopefully will there be similar initiatives globally that can increase both the number of datapoints for higher confidence in super-rare variants and for better inclusion and coverage of the human diversity. Recently, the Finnish FinnGen genotype-disease association dataset was published [76], which is a promising complementary resource to Genebass.

Taken together, we have thus confirmed the existence of germ-line activating mutations in both CARD9 and CARD10, which means that all four CARD-CC paralogs have activating mutations in the human gene pool. Many of the activating variants are in residues conserved between the CARD-CC paralogs. It is quite fascinating how residues that have remained conserved during approximately half a billion years of vertebrate evolution can be mutated and inherited in small fractions of the human population. This high level of conservation does however suggest a very strong selective pressure to maintain control of CARD-CC activation, and we expect aberrant activation of any of the four CARD-CC proteins to be very detrimental and counterselected.

It would be very interesting to investigate the biological effect of expressing the activated CARD9^{G111E} mutation by knock-in mutation of the *Card9* gene in mice. Since it persists in germline in humans, we would expect that such mice would be viable. However, previous studies have shown that a CARD14 mutation (E138A) that is non-lethal and causing psoriasis in humans can be lethal in mice [77]–[79]. If the endogenous knock-in is more detrimental in mice than in humans, an alternative would be expressing them conditionally in myeloid cells using a *Rosa26*$^{lox\text{-}stop\text{-}lox}$ system in mice, similar to what has been done previously with conditional transgenic expression of CARD11^{L232LI}, CARD11$^{\Delta ID}$ or CARD14^{E138A} to study their effects in B cells and keratinocytes, respectively [78], [80], [81]. The knock-in allele could also be expressed conditionally from its native locus, like what has also been done for *Card14*^{E138A} [82]. If the activated CARD9 mouse model would show a phenotype, it might help in the identification of patients with a similar condition due to activating *CARD9* mutations which are currently being missed. If the Genebass [57] associations of fibromyalgia to CARD9^{G111E} translate to the mouse phenotype, it could become a very valuable genetic mouse model. Current fibromyalgia models rely on disease induction through physical damage and stress, and this genetic fibromyalgia model would also come with the common comorbidities IBS, constipation and depression [83]. While fibromyalgia traditionally is not considered an inflammatory disease, recent findings indicate an inflammatory component — especially associated to hyperactivated monocytes [84], [85]. Surprisingly, clinical trials focusing on the psychological aspects of the disease are showing good results [86], [87], which could be a counterargument against a purely somatic cause for the disease. A good mouse model might also help establish whether the higher disease incidence in women is due to sex or gender [61], [83], [88]. We have already observed another sexual dimorphism in a CBM dependent autoimmune disease in MALT1 protease-dead knock in mice, resulting in gastritis, salivary- and lacrimal gland inflammation and neuroinflammation, which confirmed already known differences between men and women [89]. The IBS with constipation (IBS-C) association to CARD9^{G111E} is more expected since altered gut mycobiota and

a link between enhanced Dectin-1 signaling via CARD9 in mast cells has already been suggested to be responsible for IBS and visceral hypersensitivity [90], [91]. β-Glucan stimulation has also been implicated in development of gastrointestinal and rheumatological symptoms, indicating a role for activated CARD9 [92]. CARD9 loss-of-function mutants have an altered microbiota leading to reduced tryptophan metabolism into the phytohormone auxin (indole-3-acetic acid (IAA)) [93], [94]. Gnotobiotic mouse models using microbiota from IBS patients have shown enhanced IAA production that is also linked to anxiety and cognitive impairment [95]–[97], which might indicate that the psychological and psychosomatic disease associations seen in CARD9^{G111E} are driven by the gut. The CARD9^{G111E} mouse model would also be a valuable model to investigate targeted treatments against this disease complex and the associated gut-brain axis complications. Therapies could focus on targeting the CBM-9 complex directly via MALT1 protease inhibition [98] or CARD9-TRIM62 inhibition [72] — or by targeting the downstream gut dysbiosis and the associated enhanced tryptophan metabolism with for example the probiotic *Saccharomyces boulardii* [95], ampicillin for specific depletion of tryptophan-metabolizing bacteria [99], or inhibition of the main receptor for tryptophan metabolites – AhR [100].
The functional verification of the activating *Card10*^{R212H} mutation in using knock-in mice would also be highly interesting. Since so many POAG-associated CARD10 mutants did not show any signs of activation, we would expect other phenotypes in addition to POAG in this model. The activated *Card10* knock-in mouse model could thus also provide a valuable novel model to investigate the effects of hyperactive CARD10 in other diseases, such as cancer, asthma, liver- and lung fibrosis [101]–[104]. Some additional Genebass [57] associations for this natural CARD10^{R212H} variant (22-37516037-C-T; allergy, arthritis, cardiovascular disease, cancer), which partially overlap with the phenotypes associated to the MALT1 cleavage resistant CARD10 R587 variants, indicate that such phenotypes may be likely. Of special interest in this model will be the analysis of kidney function since this is a common disease association of the activated CARD10^{R212H} and CARD10^{R153P} variants. The availability of public exome data from biobanks with disease associations and other metadata gives unprecedented opportunities for reverse genetics approaches to find novel disease-associated mutations. We can now first establish the function of a natural variant *in vitro* and then determine the phenotypic consequences and relevance of that activity via searches in public disease association databases. It is possible that traditional forward genetics approaches would have been unable to identify the activated CARD9 and CARD10 mutations due to their rarity and associations to complex disease phenotypes.

Material and Methods

Biological material availability

All plasmid constructs used and generated in this study are available via BCCM/GeneCorner (www.genecorner.ugent.be) and can be found back using the catalog (LMBP) numbers.

Sequence and structure comparisons

Sequence analysis, alignments and primer design was done in UGene [105] installed via

BioArchLinux [106]. Protein coordinates were collected from Uniprot [56], and the coordinates were subsequently verified using Alphafold [63]. Protein structure model (pdb) files were opened in PyMOL [107] to generate the graphical snapshots used in Figure 1. The start of mCard10 PDZ domain was identified by graphical investigation in Alphafold only since it was not annotated in Uniprot.

Cloning hybrid chimeric CARD-CC fusion proteins and other mutants

In order to obtain completely scar-free fusion proteins, we employed NEBuilder (New England Biolabs) to fuse PCR products. PCR fragments were amplified using Phusion DNA polymerase (New England Biolabs) using the generic protocol and 30 s/Kb extension. Our general strategy was to amplify half of the plasmid starting from the middle of the ampicilin resistance gene and the part of the CARD-CC protein that we wanted to fuse, and then fuse the two halves of the plasmid using NEBuilder. For an overview of primers used, see (table 2), and for an overview of constructs generated, see (table 3). Original templates used for the PCR were pCDNA3-F-hCARD9 (LMBP 09609), pCDNA3-F-mCard10 (LMBP 10187), pCD-F-bio-mCard11 (LMBP 10717), pCD-F-bio-mCard11-L232LI (LMBP 07889), pCDNA3-F-hCARD14 (LMBP 09869), pCDNA3-F-hCARD14-E138A (LMBP 09860). The most optimal CARD14 Franken-CARD9 variants (C9-14L and C9-14CC) were utilized to quantitatively investigate several known psoriasis-associated mutants (table 4), which were introduced by amplification of the plasmid with the indicated mutation primers followed by DpnI (Promega) digestion. The CARD10 R404W, R420C, ΔK272-E273 and ΔK272-V277 (table 4) mutations [41]–[43] were also tested in the C9-10CC backbone using the same strategy. For future simplification of high-throughput mutagenesis, C9-14L (LMBP 13438), C9-14CC (LMBP 13437) and C9-10CC (LMBP 13439) were also re-cloned into the pICOz [108] (LMBP 11103) backbone. All the generated clones were verified using Sanger sequencing (Mix2Seq ON, Eurofins Genomics).

Other CARD-CC protein plasmid resources

Already cloned [2], [33] constructs used in this study are pCDNA3-Flag-hCARD9-L213LI (LMBP 10178), pCDNA3-Flag-hCARD9ΔC (“9N”, LMBP 10457), pCDNA3-F-mCard10ΔC (“10N”, LMBP 10459), pCD-F-bio-mCard11ΔC (“11N”, LMBP 10458) and pCDNA3-F-hCARD14ΔC (“14N”, LMBP 10460).

NF-κB luciferase analysis

For each set-up, we made a master mix of 200 ng/µg CARD-CC expression clone, 100 ng/µg NF-κB-dependent luciferase expression vector (LMBP 3249) [109], 100 ng/µg actin-promoter driven β-galactosidase (LacZ) expression plasmid (LMBP 4341) [110] and 600 ng/µg empty vector (LMBP 2453). 1 µg master mix was used to transfect 4 wells in a 24-well plate of HEK293T cells (200 000 cells/well) using the calcium phosphate transfection method. Each experiment repeated at least 3 times and a representative result presented with error bars for the technical replicates 1 standard deviation.

Western blot analysis

To ensure that the chimeric CARD-CC proteins are expressed, we lysed a set of transfected cells in Laemmli buffer [111], ran the samples on SDS-PAGE, and subsequently blotted the proteins on PVDF membranes by wet blotting. Since all the cloned CARD-CC proteins are N-terminally flag-tagged, we developed the blots using anti-Flag (clone M2, F-3165, Sigma) and detected them on an Amersham Imager 600, as loading control, we developed for anti-actin (sc-47778, Santa cruz).

Author contributions

Y.D, Ji.S, F.V.G and Je.S performed experiments. Je.S. conceptualized, planned and wrote the manuscript. Je.S and R.B. supervised the project.

Acknowledgements

Research in the authors' lab is supported by a VIB Grand Challenges grant (GC01-C01), the Fund for Scientific Research Flanders (FWO;3G086521), an Excellence of Science (EOS) research grant (3G0I1422), Ghent University Concerted Research Actions (GOA; 01G00419). F.V.G. holds a PhD fellowship strategic basic research from the FWO. Je.S. holds a doctoral assistant mandate and assistant professorship from Ghent University. Disease associations have been conducted using summary statistics generated from the UK Biobank resource (under application 26041 and 48511).

References

[1] A. Demeyer, J. Staal, and R. Beyaert, "Targeting MALT1 Proteolytic Activity in Immunity, Inflammation and Disease: Good or Bad?," *Trends Mol. Med.*, vol. 22, no. 2, pp. 135–150, Feb. 2016, doi: 10.1016/j.molmed.2015.12.004.

[2] J. Staal *et al.*, "Ancient Origin of the CARD–Coiled Coil/Bcl10/MALT1-Like Paracaspase Signaling Complex Indicates Unknown Critical Functions," *Front. Immunol.*, vol. 9, p. 1136, 2018, doi: 10.3389/fimmu.2018.01136.

[3] P. Hulpiau, Y. Driege, J. Staal, and R. Beyaert, "MALT1 is not alone after all: identification of novel paracaspases," *Cell. Mol. Life Sci. CMLS*, vol. 73, no. 5, pp. 1103–1116, Mar. 2016, doi: 10.1007/s00018-015-2041-9.

[4] A. Rodriguez Gama, T. Miller, J. J. Lange, J. R. Unruh, and R. Halfmann, "A nucleation barrier spring-loads the CBM signalosome for binary activation," *eLife*, vol. 11, p. e79826, Jun. 2022, doi: 10.7554/eLife.79826.

[5] M. Juilland and M. Thome, "Holding All the CARDs: How MALT1 Controls CARMA/CARD-Dependent Signaling," *Front. Immunol.*, vol. 9, p. 1927, 2018, doi: 10.3389/fimmu.2018.01927.

[6] J. Ruland and L. Hartjes, "CARD–BCL-10–MALT1 signalling in protective and pathological immunity," *Nat. Rev. Immunol.*, p. 1, Nov. 2018, doi: 10.1038/s41577-018-0087-2.

[7] T. Gehring, T. Seeholzer, and D. Krappmann, "BCL10 – Bridging CARDs to Immune Activation," *Front. Immunol.*, vol. 0, 2018, doi: 10.3389/fimmu.2018.01539.

[8] H. Braun and J. Staal, "Stabilization of the TAK1 adaptor proteins TAB2 and TAB3 is critical for optimal NF-κB activation," *FEBS J.*, p. doi:10.1111/febs.15210, 2020, doi: 10.1111/febs.15210.

[9] A. Garcia-Concejo and D. Larhammar, “Protein kinase C family evolution in jawed vertebrates,” *Dev. Biol.*, vol. 479, pp. 77–90, Nov. 2021, doi: 10.1016/j.ydbio.2021.07.013.
[10] A. de Mendoza, H. Suga, and I. Ruiz-Trillo, “Evolution of the MAGUK protein gene family in premetazoan lineages,” *BMC Evol. Biol.*, vol. 10, p. 93, 2010, doi: 10.1186/1471-2148-10-93.
[11] J. Staal *et al.*, “Defining the combinatorial space of PKC::CARD-CC signal transduction nodes,” *FEBS J.*, vol. 288, no. 5, pp. 1630–1647, 2021, doi: https://doi.org/10.1111/febs.15522.
[12] Q. Qiao *et al.*, “Structural Architecture of the CARMA1/Bcl10/MALT1 Signalosome: Nucleation-Induced Filamentous Assembly,” *Mol. Cell*, vol. 51, no. 6, pp. 766–779, Sep. 2013, doi: 10.1016/j.molcel.2013.08.032.
[13] F. Schlauderer *et al.*, “Molecular architecture and regulation of BCL10-MALT1 filaments,” *Nat. Commun.*, vol. 9, no. 1, p. 4041, Oct. 2018, doi: 10.1038/s41467-018-06573-8.
[14] M. J. Tanner, W. Hanel, S. L. Gaffen, and X. Lin, “CARMA1 coiled-coil domain is involved in the oligomerization and subcellular localization of CARMA1 and is required for T cell receptor-induced NF-kappaB activation,” *J. Biol. Chem.*, vol. 282, no. 23, pp. 17141–17147, Jun. 2007, doi: 10.1074/jbc.M700169200.
[15] M. J. Holliday *et al.*, “Structures of autoinhibited and polymerized forms of CARD9 reveal mechanisms of CARD9 and CARD11 activation,” *Nat. Commun.*, vol. 10, no. 1, p. 3070, Jul. 2019, doi: 10.1038/s41467-019-10953-z.
[16] J. Bertin *et al.*, “CARD9 is a novel caspase recruitment domain-containing protein that interacts with BCL10/CLAP and activates NF-kappa B,” *J. Biol. Chem.*, vol. 275, no. 52, pp. 41082–41086, Dec. 2000, doi: 10.1074/jbc.C000726200.
[17] T. Che, Y. You, D. Wang, M. J. Tanner, V. M. Dixit, and X. Lin, “MALT1/paracaspase is a signaling component downstream of CARMA1 and mediates T cell receptor-induced NF-kappaB activation,” *J. Biol. Chem.*, vol. 279, no. 16, pp. 15870–15876, Apr. 2004, doi: 10.1074/jbc.M310599200.
[18] L. M. McAllister-Lucas *et al.*, “CARMA3/Bcl10/MALT1-dependent NF-kappaB activation mediates angiotensin II-responsive inflammatory signaling in nonimmune cells,” *Proc Natl Acad Sci U A*, vol. 104, no. 1, pp. 139–44, Jan. 2007.
[19] I. S. Afonina *et al.*, “The paracaspase MALT1 mediates CARD14-induced signaling in keratinocytes,” *EMBO Rep.*, vol. 17, no. 6, pp. 914–927, Jun. 2016, doi: 10.15252/embr.201642109.
[20] E. A. Minina *et al.*, “Classification and nomenclature of metacaspases and paracaspases: no more confusion with caspases,” *Mol. Cell*, vol. 77, no. 5, pp. 927–929, 2020.
[21] P. A. Bell *et al.*, “Integrating knowledge of protein sequence with protein function for the prediction and validation of new MALT1 substrates,” *Comput. Struct. Biotechnol. J.*, Aug. 2022, doi: 10.1016/j.csbj.2022.08.021.
[22] T. Seeholzer *et al.*, “BCL10-CARD11 Fusion Mimics an Active CARD11 Seed That Triggers Constitutive BCL10 Oligomerization and Lymphocyte Activation,” *Front. Immunol.*, vol. 9, p. 2695, 2018, doi: 10.3389/fimmu.2018.02695.
[23] R. L. Lamason, R. R. McCully, S. M. Lew, and J. L. Pomerantz, “Oncogenic CARD11 mutations induce hyperactive signaling by disrupting autoinhibition by the PKC-responsive inhibitory domain,” *Biochemistry*, vol. 49, no. 38, pp. 8240–8250, Sep. 2010, doi: 10.1021/bi101052d.
[24] A. Howes *et al.*, “Psoriasis mutations disrupt CARD14 autoinhibition promoting BCL10-MALT1-dependent NF-κB activation,” *Biochem. J.*, p. BCJ20160270, Apr. 2016, doi: 10.1042/BCJ20160270.
[25] K. Sommer *et al.*, “Phosphorylation of the CARMA1 linker controls NF-kappaB activation,” *Immunity*, vol. 23, no. 6, pp. 561–574, Dec. 2005, doi: 10.1016/j.immuni.2005.09.014.
[26] M. Lork, J. Staal, and R. Beyaert, “Ubiquitination and phosphorylation of the CARD11-BCL10-

MALT1 signalosome in T cells," *Cell. Immunol.*, vol. 340, p. 103877, Jun. 2019, doi: 10.1016/j.cellimm.2018.11.001.

[27] S. B. DeVore and G. K. Khurana Hershey, "The role of the CBM complex in allergic inflammation and disease," *J. Allergy Clin. Immunol.*, pp. S0091-6749(22)00915–0, Aug. 2022, doi: 10.1016/j.jaci.2022.06.023.

[28] P. Stepensky *et al.*, "Deficiency of caspase recruitment domain family, member 11 (CARD11), causes profound combined immunodeficiency in human subjects," *J. Allergy Clin. Immunol.*, vol. 131, no. 2, pp. 477-485.e1, Feb. 2013, doi: 10.1016/j.jaci.2012.11.050.

[29] J. A. Altin, L. Tian, A. Liston, E. M. Bertram, C. C. Goodnow, and M. C. Cook, "Decreased TCR signaling through Card11 differentially compromises Foxp3+ regulatory versus Th2 effector cells to cause allergy," *J. Allergy Clin. Immunol.*, vol. 127, no. 5, pp. 1277–85.e5, May 2011, doi: 10.1016/j.jaci.2010.12.1081.

[30] C. A. Ma *et al.*, "Germline hypomorphic CARD11 mutations in severe atopic disease," *Nat. Genet.*, vol. 49, no. 8, pp. 1192–1201, Aug. 2017, doi: 10.1038/ng.3898.

[31] A. Demeyer *et al.*, "MALT1-deficient mice develop atopic-like dermatitis upon aging," *Front. Immunol.*, vol. 10, p. 2330, 2019, doi: 10.3389/fimmu.2019.02330.

[32] W. Hu, Z. Ye, P. Li, Y. Wang, and Y. Huang, "Very Early Onset Inflammatory Bowel Disease Caused by a Novel Dominant Negative Mutation of Caspase Recruitment Domain 11 (CARD11)," *J. Clin. Immunol.*, Nov. 2022, doi: 10.1007/s10875-022-01387-2.

[33] M. De Bruyne *et al.*, "A CARD9 founder mutation disrupts NF-κB signaling by inhibiting BCL10 and MALT1 recruitment and signalosome formation," *Front. Immunol.*, vol. 9, p. 2366, 2018, doi: 10.3389/fimmu.2018.02366.

[34] C. Ji, Z. Yang, X. Zhong, and J. Xia, "The role and mechanism of CARD9 gene polymorphism in diseases," *Biomed. J.*, vol. 44, no. 5, pp. 560–566, Oct. 2021, doi: 10.1016/j.bj.2020.12.006.

[35] M. Chiriaco *et al.*, "First Case of Patient With Two Homozygous Mutations in MYD88 and CARD9 Genes Presenting With Pyogenic Bacterial Infections, Elevated IgE, and Persistent EBV Viremia," *Front. Immunol.*, vol. 10, p. 130, Feb. 2019, doi: 10.3389/fimmu.2019.00130.

[36] X. Xu *et al.*, "CARD9S12N facilitates the production of IL-5 by alveolar macrophages for the induction of type 2 immune responses," *Nat. Immunol.*, vol. 19, no. 6, pp. 547–560, Jun. 2018, doi: 10.1038/s41590-018-0112-4.

[37] M. Desjardins *et al.*, "A Unique Heterozygous CARD11 Mutation Combines Pathogenic Features of Both Gain- and Loss-of-Function Patients in a Four-Generation Family," *Front. Immunol.*, vol. 9, 2018, doi: 10.3389/fimmu.2018.02944.

[38] A. Peled *et al.*, "Loss-of-function mutations in caspase recruitment domain-containing protein 14 (CARD14) are associated with a severe variant of atopic dermatitis," *J. Allergy Clin. Immunol.*, vol. 143, no. 1, pp. 173-181.e10, Jan. 2019, doi: 10.1016/j.jaci.2018.09.002.

[39] B. C. Grabiner *et al.*, "CARMA3 deficiency abrogates G protein-coupled receptor-induced NF-{kappa}B activation," *Genes Dev.*, vol. 21, no. 8, pp. 984–996, Apr. 2007, doi: 10.1101/gad.1502507.

[40] J. Ruland *et al.*, "Bcl10 is a positive regulator of antigen receptor-induced activation of NF-kappaB and neural tube closure," *Cell*, vol. 104, no. 1, pp. 33–42, Jan. 2001.

[41] D. Yang *et al.*, "Mutant CARD10 in a family with progressive immunodeficiency and autoimmunity," *Cell. Mol. Immunol.*, vol. 17, no. 7, Art. no. 7, Jul. 2020, doi: 10.1038/s41423-020-0423-x.

[42] T. Zhou *et al.*, "Rare variants in optic disc area gene CARD10 enriched in primary open-angle glaucoma," *Mol. Genet. Genomic Med.*, vol. 4, no. 6, pp. 624–633, 2016, doi: 10.1002/mgg3.248.

[43] Y. Zou *et al.*, "Analysis of CARD10 and CARD11 somatic mutations in patients with ovarian endometriosis," *Oncol. Lett.*, vol. 16, no. 1, pp. 491–496, Jul. 2018, doi: 10.3892/ol.2018.8659.

[44] S. Zhang, D. Pan, X.-M. Jia, X. Lin, and X. Zhao, “The CARMA3-BCL10-MALT1 (CBM) complex contributes to DNA damage-induced NF-κB activation and cell survival,” *Protein Cell*, pp. 1–5, Jul. 2017, doi: 10.1007/s13238-017-0441-3.
[45] D. Vanneste *et al.*, “CARD14 Signalling Ensures Cell Survival and Cancer Associated Gene Expression in Prostate Cancer Cells,” *Biomedicines*, vol. 10, no. 8, Art. no. 8, Aug. 2022, doi: 10.3390/biomedicines10082008.
[46] J. Zhang *et al.*, “Genetic heterogeneity of diffuse large B-cell lymphoma,” *Proc. Natl. Acad. Sci. U. S. A.*, vol. 110, no. 4, pp. 1398–1403, Jan. 2013, doi: 10.1073/pnas.1205299110.
[47] A. S. Brohl *et al.*, “Germline CARD11 mutation in a patient with severe congenital B cell lymphocytosis,” *J. Clin. Immunol.*, vol. 35, no. 1, pp. 32–46, Jan. 2015, doi: 10.1007/s10875-014-0106-4.
[48] L. Israel and M. Mellett, “Clinical and Genetic Heterogeneity of CARD14 Mutations in Psoriatic Skin Disease,” *Front. Immunol.*, vol. 9, p. 2239, Oct. 2018, doi: 10.3389/fimmu.2018.02239.
[49] D. Powell, “Chimera Contemporary: The Enduring Art of the Composite Beast,” *Leonardo*, vol. 37, no. 4, pp. 332–340, Aug. 2004, doi: 10.1162/0024094041724472.
[50] B. Cohen, “New light on a master bronze from Etruria,” *Online Mus. Rev. AJA*, vol. 114, no. 3, pp. 1–10, 2010, doi: 10.3764/ajaonline1143.Cohen.
[51] Y. Nakatani *et al.*, “Reconstruction of proto-vertebrate, proto-cyclostome and proto-gnathostome genomes provides new insights into early vertebrate evolution,” *Nat. Commun.*, vol. 12, no. 1, Art. no. 1, Jul. 2021, doi: 10.1038/s41467-021-24573-z.
[52] A. L. Snow *et al.*, “Congenital B cell lymphocytosis explained by novel germline CARD11 mutations,” *J. Exp. Med.*, vol. 209, no. 12, pp. 2247–2261, Nov. 2012, doi: 10.1084/jem.20120831.
[53] G. Lenz *et al.*, “Oncogenic CARD11 mutations in human diffuse large B cell lymphoma,” *Science*, vol. 319, no. 5870, pp. 1676–1679, Mar. 2008, doi: 10.1126/science.1153629.
[54] W. Chan, T. B. Schaffer, and J. L. Pomerantz, “A Quantitative Signaling Screen Identifies CARD11 Mutations in the CARD and LATCH Domains That Induce Bcl10 Ubiquitination and Human Lymphoma Cell Survival,” *Mol. Cell. Biol.*, vol. 33, no. 2, pp. 429–443, Jan. 2013, doi: 10.1128/MCB.00850-12.
[55] D. Strasser *et al.*, “Syk kinase-coupled C-type lectin receptors engage protein kinase C-σ to elicit Card9 adaptor-mediated innate immunity,” *Immunity*, vol. 36, no. 1, pp. 32–42, Jan. 2012, doi: 10.1016/j.immuni.2011.11.015.
[56] The UniProt Consortium, “UniProt: the universal protein knowledgebase in 2021,” *Nucleic Acids Res.*, vol. 49, no. D1, pp. D480–D489, Jan. 2021, doi: 10.1093/nar/gkaa1100.
[57] K. J. Karczewski *et al.*, “Systematic single-variant and gene-based association testing of thousands of phenotypes in 394,841 UK Biobank exomes,” *Cell Genomics*, vol. 2, no. 9, p. 100168, Sep. 2022, doi: 10.1016/j.xgen.2022.100168.
[58] V. Khanijow, P. Prakash, H. A. Emsellem, M. L. Borum, and D. B. Doman, “Sleep Dysfunction and Gastrointestinal Diseases,” *Gastroenterol. Hepatol.*, vol. 11, no. 12, pp. 817–825, Dec. 2015.
[59] E. Axelsson, M. Hedman-Lagerlöf, E. Hedman-Lagerlöf, B. Ljótsson, and E. Andersson, “Symptom Preoccupation in Fibromyalgia: Prevalence and Correlates of Somatic Symptom Disorder in a Self-Recruited Sample,” *Psychosomatics*, vol. 61, no. 3, pp. 268–276, May 2020, doi: 10.1016/j.psym.2020.01.012.
[60] S. Erdrich, J. A. Hawrelak, S. P. Myers, and J. E. Harnett, “A systematic review of the association between fibromyalgia and functional gastrointestinal disorders,” *Ther. Adv. Gastroenterol.*, vol. 13, p. 1756284820977402, Dec. 2020, doi: 10.1177/1756284820977402.
[61] F. Bonfiglio *et al.*, “Female-Specific Association Between Variants on Chromosome 9 and Self-Reported Diagnosis of Irritable Bowel Syndrome,” *Gastroenterology*, vol. 155, no. 1, pp. 168–179, Jul. 2018, doi: 10.1053/j.gastro.2018.03.064.

[62] K. J. Karczewski *et al.*, “The mutational constraint spectrum quantified from variation in 141,456 humans,” *Nature*, vol. 581, no. 7809, Art. no. 7809, May 2020, doi: 10.1038/s41586-020-2308-7.
[63] J. Jumper *et al.*, “Highly accurate protein structure prediction with AlphaFold,” *Nature*, vol. 596, no. 7873, pp. 583–589, Aug. 2021, doi: 10.1038/s41586-021-03819-2.
[64] C. T. Jordan *et al.*, “PSORS2 is due to mutations in CARD14,” *Am. J. Hum. Genet.*, vol. 90, no. 5, pp. 784–795, May 2012, doi: 10.1016/j.ajhg.2012.03.012.
[65] P. Ekambaram *et al.*, “The CARMA3-Bcl10-MALT1 Signalosome Drives NFκB Activation and Promotes Aggressiveness in Angiotensin II Receptor-Positive Breast Cancer,” *Cancer Res.*, vol. 78, no. 5, pp. 1225–1240, Mar. 2018, doi: 10.1158/0008-5472.CAN-17-1089.
[66] H. Zhang *et al.*, “PIM1 genetic alterations associated with distinct molecular profiles, phenotypes and drug responses in diffuse large B-cell lymphoma,” *Clin. Transl. Med.*, vol. 12, no. 4, Apr. 2022, doi: 10.1002/ctm2.808.
[67] B. Han, S. Kim, J. Koh, J. M. Bae, H. Yun, and Y. K. Jeon, “An unusual case of microsatellite instability–high/deficient mismatch repair (MSI-H/dMMR) diffuse large B-cell lymphoma revealed by targeted gene sequencing,” *J. Pathol. Transl. Med.*, vol. 56, no. 2, pp. 92–96, Mar. 2022, doi: 10.4132/jptm.2021.10.15.
[68] T. Pieters *et al.*, “Cyclin D2 overexpression drives B1a-derived MCL-like lymphoma in mice,” *J. Exp. Med.*, vol. 218, no. 10, Aug. 2021, doi: 10.1084/jem.20202280.
[69] L. Fontan *et al.*, “MALT1 small molecule inhibitors specifically suppress ABC-DLBCL in vitro and in vivo,” *Cancer Cell*, vol. 22, no. 6, pp. 812–824, Dec. 2012, doi: 10.1016/j.ccr.2012.11.003.
[70] C.-H. Yang and C. Zwieb, “Swapping of Functional Domains Using a Chimeric Monster Deletion Mutagenesis Strategy,” *BioTechniques*, vol. 31, no. 4, pp. 724–728, Oct. 2001, doi: 10.2144/01314bm02.
[71] N. Ferruz, J. Noske, and B. Höcker, “Protlego: a Python package for the analysis and design of chimeric proteins,” *Bioinformatics*, vol. 37, no. 19, pp. 3182–3189, Oct. 2021, doi: 10.1093/bioinformatics/btab253.
[72] E. S. Leshchiner *et al.*, “Small-molecule inhibitors directly target CARD9 and mimic its protective variant in inflammatory bowel disease,” *Proc. Natl. Acad. Sci. U. S. A.*, vol. 114, no. 43, pp. 11392–11397, Oct. 2017, doi: 10.1073/pnas.1705748114.
[73] Z. Cao *et al.*, “The Ubiquitin Ligase TRIM62 Regulates CARD9-Mediated Anti-Fungal Immunity and Intestinal Inflammation,” *Immunity*, vol. 43, no. 4, pp. 715–726, Oct. 2015, doi: 10.1016/j.immuni.2015.10.005.
[74] L. Israël *et al.*, “CARD10 cleavage by MALT1 restricts lung carcinoma growth in vivo,” *Oncogenesis*, vol. 10, no. 4, p. 32, Apr. 2021, doi: 10.1038/s41389-021-00321-2.
[75] J. Staal, “Applied Cultural and Social Studies are Needed for a Sustainable Reduction of Genetic Disease Incidence,” *Eur. J. Sociol. Anthropol.*, vol. 2, no. 1, p. 1, Jun. 2017, doi: 10.20897/ejsa.201701.
[76] M. I. Kurki *et al.*, “FinnGen provides genetic insights from a well-phenotyped isolated population,” *Nature*, vol. 613, no. 7944, Art. no. 7944, Jan. 2023, doi: 10.1038/s41586-022-05473-8.
[77] M. Wang *et al.*, “Gain-of-Function Mutation of Card14 Leads to Spontaneous Psoriasis-like Skin Inflammation through Enhanced Keratinocyte Response to IL-17A,” *Immunity*, vol. 49, no. 1, pp. 66-79.e5, Jul. 2018, doi: 10.1016/j.immuni.2018.05.012.
[78] E. Van Nuffel *et al.*, “MALT1 targeting suppresses CARD14-induced psoriatic dermatitis in mice,” *EMBO Rep.*, vol. 21, no. 7, p. e49237, Jul. 2020, doi: 10.15252/embr.201949237.
[79] J. P. Sundberg *et al.*, “Gain of function p.E138A alteration in Card14 leads to psoriasiform skin inflammation and implicates genetic modifiers in disease severity,” *Exp. Mol. Pathol.*, vol. 110,

p. 104286, Oct. 2019, doi: 10.1016/j.yexmp.2019.104286.
[80] M. K. Bognar *et al.*, “Oncogenic CARMA1 couples NF-κB and β-catenin signaling in diffuse large B-cell lymphomas,” *Oncogene*, vol. 35, no. 32, pp. 4269–4281, Aug. 2016, doi: 10.1038/onc.2015.493.
[81] Z. Kurgyis *et al.*, “Keratinocyte-intrinsic BCL10/MALT1 activity initiates and amplifies psoriasiform skin inflammation,” *Sci. Immunol.*, vol. 6, no. 65, p. eabi4425, Nov. 2021, doi: 10.1126/sciimmunol.abi4425.
[82] J. Manils *et al.*, “CARD14E138A signalling in keratinocytes induces TNF-dependent skin and systemic inflammation,” *eLife*, vol. 9, p. e56720, Jun. 2020, doi: 10.7554/eLife.56720.
[83] E. S. Brum, G. Becker, M. F. P. Fialho, and S. M. Oliveira, “Animal models of fibromyalgia: What is the best choice?,” *Pharmacol. Ther.*, vol. 230, p. 107959, Feb. 2022, doi: 10.1016/j.pharmthera.2021.107959.
[84] E. N. Merriwether *et al.*, “IL-5 mediates monocyte phenotype and pain outcomes in fibromyalgia,” *Pain*, vol. 162, no. 5, pp. 1468–1482, May 2021, doi: 10.1097/j.pain.0000000000002089.
[85] E. Bäckryd, L. Tanum, A.-L. Lind, A. Larsson, and T. Gordh, “Evidence of both systemic inflammation and neuroinflammation in fibromyalgia patients, as assessed by a multiplex protein panel applied to the cerebrospinal fluid and to plasma,” *J. Pain Res.*, vol. 10, pp. 515–525, Mar. 2017, doi: 10.2147/JPR.S128508.
[86] D. Maroti *et al.*, “Internet-Administered Emotional Awareness and Expression Therapy for Somatic Symptom Disorder With Centralized Symptoms: A Preliminary Efficacy Trial,” *Front. Psychiatry*, vol. 12, 2021, Accessed: Oct. 23, 2022. [Online]. Available: https://www.frontiersin.org/articles/10.3389/fpsyt.2021.620359
[87] B. Ljótsson *et al.*, “Internet-Delivered Acceptance and Values-Based Exposure Treatment for Fibromyalgia: A Pilot Study,” *Cogn. Behav. Ther.*, vol. 43, no. 2, pp. 93–104, Apr. 2014, doi: 10.1080/16506073.2013.846401.
[88] N. Z. Gungor, A. Duchesne, and R. Bluhm, “A conversation around the integration of sex and gender when modeling aspects of fear, anxiety, and PTSD in animals,” *SF Online*, vol. 15, no. 2, 2019.
[89] A. Demeyer *et al.*, “MALT1 Proteolytic Activity Suppresses Autoimmunity in a T Cell Intrinsic Manner,” *Front. Immunol.*, vol. 10, p. 1898, 2019, doi: 10.3389/fimmu.2019.01898.
[90] Y. Chi, C. Li, L.-H. Wu, and H.-H. Wang, “The relationship between dectin-1 and mast cells in patients with diarrhea-predominant irritable bowel syndrome,” *Scand. J. Gastroenterol.*, vol. 55, no. 7, pp. 762–768, Jul. 2020, doi: 10.1080/00365521.2020.1774925.
[91] A. Liu, W. Gao, Y. Zhu, X. Hou, and H. Chu, “Gut Non-Bacterial Microbiota: Emerging Link to Irritable Bowel Syndrome,” *Toxins*, vol. 14, no. 9, p. 596, Aug. 2022, doi: 10.3390/toxins14090596.
[92] M. Ruutu *et al.*, “β-glucan triggers spondylarthritis and Crohn’s disease-like ileitis in SKG mice,” *Arthritis Rheum.*, vol. 64, no. 7, pp. 2211–2222, Jul. 2012, doi: 10.1002/art.34423.
[93] B. Lamas *et al.*, “CARD9 impacts colitis by altering gut microbiota metabolism of tryptophan into aryl hydrocarbon receptor ligands,” *Nat. Med.*, vol. 22, no. 6, Art. no. 6, Jun. 2016, doi: 10.1038/nm.4102.
[94] C. Danne *et al.*, “Dissecting the respective roles of microbiota and host genetics in the susceptibility of Card9-/- mice to colitis.” bioRxiv, p. 2023.01.03.522555, Jan. 03, 2023. doi: 10.1101/2023.01.03.522555.
[95] M. Constante *et al.*, “Saccharomyces boulardii CNCM I-745 modulates the microbiota-gut-brain axis in a humanized mouse model of Irritable Bowel Syndrome,” *Neurogastroenterol. Motil. Off. J. Eur. Gastrointest. Motil. Soc.*, vol. 33, no. 3, p. e13985, Mar. 2021, doi: 10.1111/nmo.13985.
[96] S. W. Kim, A. Goossens, C. Libert, F. Van Immerseel, J. Staal, and R. Beyaert,

"Phytohormones: Multifunctional nutraceuticals against metabolic syndrome and comorbid diseases," *Biochem. Pharmacol.*, p. 113866, Feb. 2020, doi: 10.1016/j.bcp.2020.113866.

[97] A. M. Plantinga *et al.*, "Exploration of associations among dietary tryptophan, microbiome composition and function, and symptom severity in irritable bowel syndrome," *Neurogastroenterol. Motil.*, vol. n/a, no. n/a, p. e14545, doi: 10.1111/nmo.14545.

[98] I. Hamp, T. J. O'Neill, O. Plettenburg, and D. Krappmann, "A patent review of MALT1 inhibitors (2013-present)," *Expert Opin. Ther. Pat.*, vol. 31, no. 12, pp. 1079–1096, Dec. 2021, doi: 10.1080/13543776.2021.1951703.

[99] T. Zelante *et al.*, "Tryptophan Catabolites from Microbiota Engage Aryl Hydrocarbon Receptor and Balance Mucosal Reactivity via Interleukin-22," *Immunity*, vol. 39, no. 2, pp. 372–385, Aug. 2013, doi: 10.1016/j.immuni.2013.08.003.

[100] M. Modoux, N. Rolhion, S. Mani, and H. Sokol, "Tryptophan Metabolism as a Pharmacological Target," *Trends Pharmacol. Sci.*, vol. 42, no. 1, pp. 60–73, Jan. 2021, doi: 10.1016/j.tips.2020.11.006.

[101] Y. S. de Boer *et al.*, "Genome-Wide Association Study Identifies Variants Associated With Autoimmune Hepatitis Type 1," *Gastroenterology*, vol. 147, no. 2, pp. 443-452.e5, Aug. 2014, doi: 10.1053/j.gastro.2014.04.022.

[102] B. Causton *et al.*, "CARMA3 Mediates Allergic Lung Inflammation in Response to Alternaria alternata," *Am. J. Respir. Cell Mol. Biol.*, vol. 59, no. 6, pp. 684–694, Jun. 2018, doi: 10.1165/rcmb.2017-0181OC.

[103] Y. Wu, Y. Qi, Z. Qiu, and W. Chen, "Deficiency of CARMA3 attenuates the development of bleomycin induced pulmonary fibrosis," *Biochem. Biophys. Res. Commun.*, vol. 581, pp. 81–88, Dec. 2021, doi: 10.1016/j.bbrc.2021.10.013.

[104] Z. Gui, Y. Zhang, A. Zhang, W. Xia, and Z. Jia, "CARMA3: A potential therapeutic target in non-cancer diseases," *Front. Immunol.*, vol. 13, p. 1057980, Dec. 2022, doi: 10.3389/fimmu.2022.1057980.

[105] K. Okonechnikov, O. Golosova, M. Fursov, and UGENE team, "Unipro UGENE: a unified bioinformatics toolkit," *Bioinforma. Oxf. Engl.*, vol. 28, no. 8, pp. 1166–1167, Apr. 2012, doi: 10.1093/bioinformatics/bts091.

[106] G. Zhang, M. Elliot, Y. Hu, V. Drobot, J. Staal, and Y. Yi, "BioArchLinux: bioinformatics community with Arch Linux," in *Bioinformatics Open Source Conference*, 2022. doi: 10.7490/f1000research.1119039.1.

[107] Schrödinger, LLC, "The PyMOL Molecular Graphics System, Version 2.5.0," 2021.

[108] J. Staal, K. Alci, W. De Schamphelaire, M. Vanhoucke, and R. Beyaert, "Engineering a minimal cloning vector from a pUC18 plasmid backbone with an extended multiple cloning site," *BioTechniques*, vol. 66, no. 6, pp. 254–259, Jun. 2019, doi: 10.2144/btn-2019-0014.

[109] A. Kimura, A. Israël, O. Le Bail, and P. Kourilsky, "Detailed analysis of the mouse H-2Kb promoter: enhancer-like sequences and their role in the regulation of class I gene expression," *Cell*, vol. 44, no. 2, pp. 261–272, Jan. 1986, doi: 10.1016/0092-8674(86)90760-9.

[110] T. Ishida *et al.*, "Identification of TRAF6, a Novel Tumor Necrosis Factor Receptor-associated Factor Protein That Mediates Signaling from an Amino-terminal Domain of the CD40 Cytoplasmic Region," *J. Biol. Chem.*, vol. 271, no. 46, pp. 28745–28748, Nov. 1996, doi: 10.1074/jbc.271.46.28745.

[111] U. K. Laemmli, "Cleavage of Structural Proteins during the Assembly of the Head of Bacteriophage T4," *Nature*, vol. 227, no. 5259, pp. 680–685, Aug. 1970, doi: 10.1038/227680a0.

Table 1

Coordinates of the different modules used for hybrid CARD-CC proteins. We use human CARD9 and CARD14 and mouse CARD10 and CARD11 because those were available in the lab and previous work on different mutants has been done on those backbones. The sequence difference between human and mouse orthologs is very small compared to the difference between the CARD-CC paralogs, which diverged prior to the evolution of sharks. Domain coordinates were taken from Uniprot and verified or complemented by (predicted) structure investigations using Alphafold and sequence alignments. MAGUK is defined as from the start of the PDZ domain.

#	Domain	hCARD9		mCARD10		mCARD11		hCARD14	
①	N-CARD	1 [M...]	[...GKE] 98	1 [M...]	[...GQE] 115	1 [M...]	[...GKE] 110	1 [M...]	[...GLQ] 107
②	LATCH	99 [PAR...]	[...GLT] 116	116 [PAQ...]	[...GLT] 133	111 [PTR...]	[...GLT] 128	108 [PDV...]	[...KLT] 125
③	CC	117 [QLL...]	[...QLE] 419	134 [QFL...]	[...TQG] 450	129 [HFL...]	[...QSL] 449	126 [ECL...]	[...QAE] 409
④	Link/ID/Ct	420 [TLV...]	[...*] 536	451 [GSC...]	675 [...LLD]	450 [PRH...]	[...PLV] 671	410 [PPG...]	[...ILS] 567
⑤	MAGUK-C	N/A	N/A	676 [SKA...]	[...*] 1021	672 [QHT...]	[...*] 1159	568 [QVT...]	[...*] 1004

Table 2
Primers used for fusion CARD-CC proteins and mutants.

Primer	Sequence	Notes
Amp-mF	CAACAATTAATAGACTGGATGGAG	Used to amplify half the plasmid (ensure fusion)
Amp-mR	CTCCATCCAGTCTATTAATTGTTG	Used to amplify half the plasmid (ensure fusion)
hCARD9-T231P-F	GGTGGAGCGCAAGCACCCACTGAAGCTCAGG	Quickchange with reverse complement (-R) primer
hCARD9-G111E-F	GACGCGTCCGAAGAGTCAGGC	Quickchange with reverse complement (-R) primer
hCARD9-V102I-F	CAAGGAGCCGGCCCGCATATTCTCCATG	Quickchange with reverse complement (-R) primer
hCARD9-R101H-F	GGAGCCGGCCCATGTCTTCTC	Quickchange with reverse complement (-R) primer
hCARD9-Y86C-F	CTGGAGCTCTGTTACCCGCAG	Quickchange with reverse complement (-R) primer
hCARD9-L85F-F	AGCCTGGAGTTTTACTACCCG	Quickchange with reverse complement (-R) primer
mCARD11-S250P-F	GAGAGAAATCAGCCTCTCAAGCTC	Quickchange with reverse complement (-R) primer
hCARD14-S250P-F	GCAAGAGCAGCCTCTGAGGACAGC	Quickchange with reverse complement (-R) primer
x-hCARD9C-F	ACGCTCGTCCTGAGCTCCGACCTG	PCR with Amp-mF, hCARD9 ④ fragment
mCARD10N-hCARD9C-R	CAGGTCGGAGCTCAGGACGAGCGTCCCCTGTGTCCGCTGCAGCTGTGC	PCR with Amp-mR, mCard10 ③ to fuse with hCARD9 ④ fragment
mCARD11N-hCARD9C-R	CAGGTCGGAGCTCAGGACGAGCGTCAGACTCTGGTCGAGGCTGCCGTTGTC	PCR with Amp-mR, mCard11 ③ to fuse with hCARD9 ④ fragment
hCARD14N-hCARD9C-R	CAGGTCGGAGCTCAGGACGAGCGTCTCTGCCTGCAGCTGGCGAAGCTG	PCR with Amp-mR, hCARD14 ③ to fuse with hCARD9 ④ fragment
C9_CARD-R	CTCCTTGCCTGTGACCTTCTTGT	PCR with Amp-mR, hCARD9 ① fragment
C9_CARD-mC10_LCC-F	ACAAGAAGGTCACAGGCAAGGAGCCTGCCCAACGCTGCTCCATG	PCR with Amp-mF, mCard10 ② to fuse with hCARD9 ① fragment
C9_CARD_mC11_LCC-F	ACAAGAAGGTCACAGGCAAGGAGCCCACCCGGAGATTCTCCACCATTG	PCR with Amp-mF, mCard11 ② to fuse with hCARD9 ① fragment
C9_CARD_C14_LCC-F	ACAAGAAGGTCACAGGCAAGGAGCCTGATGTTGACTTCAGTAAC	PCR with Amp-mF, hCARD14 ② to fuse with hCARD9 ① fragment
CARD9_LATCH-F	CCGGCCCGCGTCTTCTCCATGATC	PCR with Amp-mF, hCARD9 ② to fuse with ① fragments
C9L_mC10-CARD-R	GATCATGGAGAAGACGCGGGCCGGTTCCTGGCCAGTGAGCAGCGTG	PCR with Amp-mR, mCard10 ① fragment
C9L_mC11-CARD-R	GATCATGGAGAAGACGCGGGCCGGTTCCTTTCCAGTCACCAGTTTG	PCR with Amp-mR, mCard11 ① fragment
C9L_hC14-CARD-R	GATCATGGAGAAGACGCGGGCCGGCTGCAGCCCGGTGACCAGGGTGTA	PCR with Amp-mR, hCARD14 ① fragment
CARD9_LATCH-R	AGTCAGGCCTGACTCCCCGGAC	PCR with Amp-mR, hCARD9 ② to fuse with ③ fragments
C9L_mC10-CC-F2	GTCCGGGGAGTCAGGCCTGACTCAGTTCTTGATGACTGAGGTC	PCR with Amp-mF, mCard10 ③ to fuse with hCARD9 ② fragment
C9L-mC11-CC-F2	GTCCGGGGAGTCAGGCCTGACTCACTTCCTGATGAACGAGGTC	PCR with Amp-mF, mCard11 ③ to fuse with hCARD9 ② fragment
C9L-hC14-CC-F3	GTCCGGGGAGTCAGGCCTGACTGAGTGCCTGGCTGGGGCCATCG	PCR with Amp-mF, hCARD14 ③ to fuse with hCARD9 ② fragment
CARD9_CC-F	CAGCTGCTGATGACTGAGGTCATG	PCR with Amp-mF, hCARD9 ③ to fuse with ② fragments

C9CC_mC10-LATCH-R2	CATGACCTCAGTCATCAGCAGCTGAGTCAGGCCCTCGGGACCCTCCT	PCR with Amp-mR, mCard10 ② to fuse with hCARD9 ③ fragment
C9CC_mC11-LATCH-R2	CATGACCTCAGTCATCAGCAGCTGTGTGAGGCCCTCATGGCCTTCCTCCA	PCR with Amp-mR, mCard11 ② to fuse with hCARD9 ③ fragment
C9CC_hC14-LATCH-R2	CATGACCTCAGTCATCAGCAGCTGGGTCAGCTTGGATGTCTCCATGAG	PCR with Amp-mR, hCARD14 ② to fuse with hCARD9 ③ fragment
mCard10-CC-end-F	AGGCACAGCTGCAGCGGACACAG	PCR with Amp-mF, mCard10 template, generate mCard10-9CL
mCard10-CC-end-R	CTGTGTCCGCTGCAGCTGTGCCT	PCR with Amp-mR, CARD9-10CC template, generate mCard10-9CL
mC10-dMAGUK-F	CTCCCCTTCCTGCTGGACtgaCGACTGTGCCTTCTAGTTGC	MAGUK deletion primer for mCard10
mC10-dMAGUK-R	GTCCAGCAGGAAGGGGAG	MAGUK deletion primer for mCard10
mC11-dMAGUK-F	CGGGGCACCGGaCCCTTGGTCtgaCGACTGTGCCTTCTAGTTGC	MAGUK deletion primer for mCard11
mC11-dMAGUK-R	GACCAAGGGtCCGGTGCCCCG	MAGUK deletion primer for mCard11
hC14-dMAGUK-F	CCAGCCCGCAGaATCCTGAGCtgaCGACTGTGCCTTCTAGTTGC	MAGUK deletion primer for hCARD14
hC14-dMAGUK-R	GCTCAGGATtCTGCGGGCTGG	MAGUK deletion primer for hCARD14
CARD14-CC-end-F :	GCTTCGCCAGCTGCAGGCAGAG	PCR with Amp-mF, CARD14 template, generate hCARD14-9C
CARD14-CC-end-R	CTCTGCCTGCAGCTGGCGAAGC	PCR with Amp-mR, CARD9-14LCC template, generate hCARD14-9C

Table 3
Overview of constructs generated in this study. Further derivative constructs made in this study can be found in table 4.

Abbreviation	LMBP	Notes (forward mutation primer)
CARD9-T231P	13279	CARD9 T231P mutant (GGTGGAGCGCAAGCACCCACTGAAGCTCAGG)
CARD9-G111E	13652	CARD9 G111E mutant (GACGCGTCCGAAGAGTCAGGC)
CARD9-V102I	13651	CARD9 V102I mutant (CAAGGAGCCGGCCCGCATATTCTCCATG)
CARD9-R101H	13653	CARD9 R101H mutant (GGAGCCGGCCCATGTCTTCTC)
CARD9-Y86C	13649	CARD9 Y86C mutant (CTGGAGCTCTGTTACCCGCAGCTGT)
CARD9-L85F	13650	CARD9 L85F mutant (AGCCTGGAGTTTTACTACCCGCAGCTGT)
CARD9-G111R	13722	CARD9 G111R mutant (GACGCGTCCCGAGAGTCAGGCCTGA)
CARD9-G111A	13729	CARD9 G111A mutant (CGACGCGTCCGCTGAGTCAGGCCT)
CARD9-K165E	13723	CARD9 K165E mutant (GTGCAGAGGCTCGAAGAGGAGTGCGAG)
CARD9-K165del	13727	CARD9 K165del mutant (GTGCAGAGGCTCGAGGAGTGCGAG)
CARD9-S172N	13724	CARD9 S172N mutant (GTGCGAGGCCGGCAATCGCGAGCTC)
CARD9-L423V	13732	CARD9 L423V mutant (GAGACGCTCGTCGTAAGCTCCGACC)
CARD9-E523Q	13725	CARD9 E523Q mutant (GGAGGAGGACCGGCAAAACACCACGG)

CARD9-E523K	13728	CARD9 E523K mutant (GAGGAGGACCGGAAGAACACCACGG)
CARD9-*537Qext59*	13719	CARD9 *537Qext59* mutant (Qext59* amplified from genomic DNA) forward: ACCGACACTGAGGGCTCCcAGCCGCAGCAGCGCAGG reverse: CTCGAGCGGCCGCTTAACAAACGGCCCCAATGCC
CARD11-S250P	13339	CARD11 S250P mutant (GAGAGAAATCAGCCTCTCAAGCTC)
CARD14-S250P	13331	CARD14 S250P mutant (GCAAGAGCAGCCTCTGAGGACAGC)
10N9C	13282	CARD-LATCH-CC from mCard10, ④ from hCARD9
11N9C	13280	CARD-LATCH-CC from mCard11, ④ from hCARD9
11N9C-L232LI	13281	CARD-LATCH-CC from mCard11-L232LI, ④ from hCARD9
14N9C	13283	CARD-LATCH-CC from hCARD14, ④ from hCARD9
14N9C-E138A	13284	CARD-LATCH-CC from hCARD14-E138A, ④ from hCARD9
C9-10LCC	13293	CARD9 with LATCH-CC from mCard10
C9-11LCC	13291	CARD9 with LATCH-CC from mCard11
C9-11LCC-L232LI	13294	CARD9 with LATCH-CC from mCard11-L232LI
C9-14LCC	13287	CARD9 with LATCH-CC from hCARD14
C9-14LCC-E138A	13288	CARD9 with LATCH-CC from hCARD14-E138A
C9-10CC	13305	CARD9 with CC from mCard10
C9-11CC	13309	CARD9 with CC from mCard11
C9-11CC-L232LI	13310	CARD9 with CC from mCard11-L232LI
C9-14CC	13346	CARD9 with CC from hCARD14
C9-14CC-E138A	13362	CARD9 with CC from hCARD14-E138A
C9-10C	13304	CARD9 with CARD from mCard10
C9-11C	13296	CARD9 with CARD from mCard11
C9-14C	13297	CARD9 with CARD from hCARD14
C9-10CL	13313	CARD9 with CARD-LATCH from mCard10
C9-11CL	13306	CARD9 with CARD-LATCH from mCard11
C9-14CL	13311	CARD9 with CARD-LATCH from hCARD14
C9-10L	13312	CARD9 with LATCH from mCard10
C9-11L	13307	CARD9 with LATCH from mCard11
C9-14L	13308	CARD9 with LATCH from hCARD14
C10-dM	13303	mCard10 with MAGUK deleted to generate CARD9-like protein
C10-9CL	13449	mCard10 with CARD-LATCH replaced by CARD9 CARD-LATCH
C11-dM	13300	mCard11 with MAGUK deleted to generate CARD9-like protein
C11-dM-L232LI	13301	mCard11-L232LI with MAGUK deleted to generate CARD9-like protein
C14-dM	13299	hCARD14 with MAGUK deleted to generate CARD9-like protein

C14-dM-E138A	13298	hCARD14-E138 with MAGUK deleted to generate CARD9-like protein
C14-9C	13448	hCARD14 with CARD domain replaced by CARD9 CARD

Table 4
Clones of published LATCH-CC-domain mutations in CARD10 and CARD14 using the minimal Franken-CARD9 backbones C9-14L, C9-14CC, C9-10L, C9-10CC and the good auto-inhibited mouse CARD10 backbone C10-9CL.

Abbreviation	Mutation primer (F)	LMBP
C9-14L	N/A	13308
C9-14L-G117S	AGTAACTTTAGCTCTCTCATGGAGA	13577
C9-14L-M119R	AGCGGTCTCCGAGAGACATCCAAGC	13578
C9-14L-M119T	AGCGGTCTCACAGAGACATCCAAGC	13579
C9-14L-M119V	AGCGGTCTCGTTGAGACATCCAAGC	13580
C9-14L-L124P	ACATCCAAGCCTACCCAGCTGCTGA	13589
C9-10L	N/A	13312
C9-10L-RVF	CCTGCCCGCGTCTTCTCCATGATCCTTG	13656
C9-10L-AS	GATCCTTGATGCGTCCGGTCCCGAGG	13672
C9-10L-ES	GATGAGGAGGGTGAGTCAGGCCTGAC	13726
C9-14CC	N/A	13346
C9-14CC-Q136L	TCGGCAGCCTGCTAGAGGAGCTGAA	13454
C9-14CC-E138A	N/A	13362
C9-14CC-E138K	AGCCTGCAGGAGAAACTGAACCAG	13453
C9-14CC-E138del	AGCCTGCAGGAGCTGAACCAGGAA	13452
C9-14CC-E142K	AGCTGAACCAGAAGAAGGGGCAGAA	13451
C9-14CC-E142G	AGCTGAACCAGGGTAAGGGGCAGAA	13450
C9-10CC	N/A	13305
C9-10CC-R212H	TGATCGCCATGCATCTGGCTCAGCT	13458
C9-10CC- ΔK272-E273	GAGGAGAAGGAGCCAGATGGCGCTG	13456
C9-10CC-ΔK272-V277	GAGGAGAAGGAGGATCTTCTCTCTG	13457
C9-10CC-A328V	ACTGGAGGGAGGTTCAGGACAGCAG	13461
C9-10CC-V342M	AGCTTCATGCTATGCAGGGCGAGCT	13455
C9-10CC-R404W	AGAGCCGAGACTGGATCCAGCTGCA	13460
C9-10CC-R420C	AGGACCAGTACTGTAAGCAGGTGC	13459
C10-9CL	N/A	13449
C10-9CL-R212H	mCard10-CC-end-R, Amp-mR, C9-10CC-R212H template	13584

C10-9CL-ΔK272-E273	mCard10-CC-end-R, Amp-mR, C9-10CC- ΔK272-E273 template	13582
C10-9CL-ΔK272-V277	mCard10-CC-end-R, Amp-mR, C9-10CC-A328V template	13583
C10-9CL-A328V	mCard10-CC-end-R, Amp-mR, C9-10CC-A328V template	13581
C10-9CL-V342M	mCard10-CC-end-R, Amp-mR, C9-10CC-V342M template	13587
C10-9CL-R404W	mCard10-CC-end-R, Amp-mR, C9-10CC-R404W template	13585
C10-9CL-R420C	mCard10-CC-end-R, Amp-mR, C9-10CC-R420C template	13586
C10-9CL-R212C	CATGATCGCCATGTGTCTGGCTCAGC	13670
C10-9CL-R212L	CATGATCGCCATGCTGCTGGCTCAGC	13671
C10-9CL-R142Q	TGAGGTCCGGCAACTTCGGGAA	13721
C10-9CL-E145K	GAGGCTTCGGAAGGCTCGGAAG	13668
C10-9CL-R153P	CAACTGCACCCTGAGCAGCAAC	13669
C10-9CL-R364Q	GGAGGATCTGCAACTCAAACATCG	13720
C10-9CL-R364W	GGAGGATCTGTGGCTCAAACATCG	13733
C10-9CL-E390A	CCAGCTGGAGGCTATTGAGAAAGAG	13734

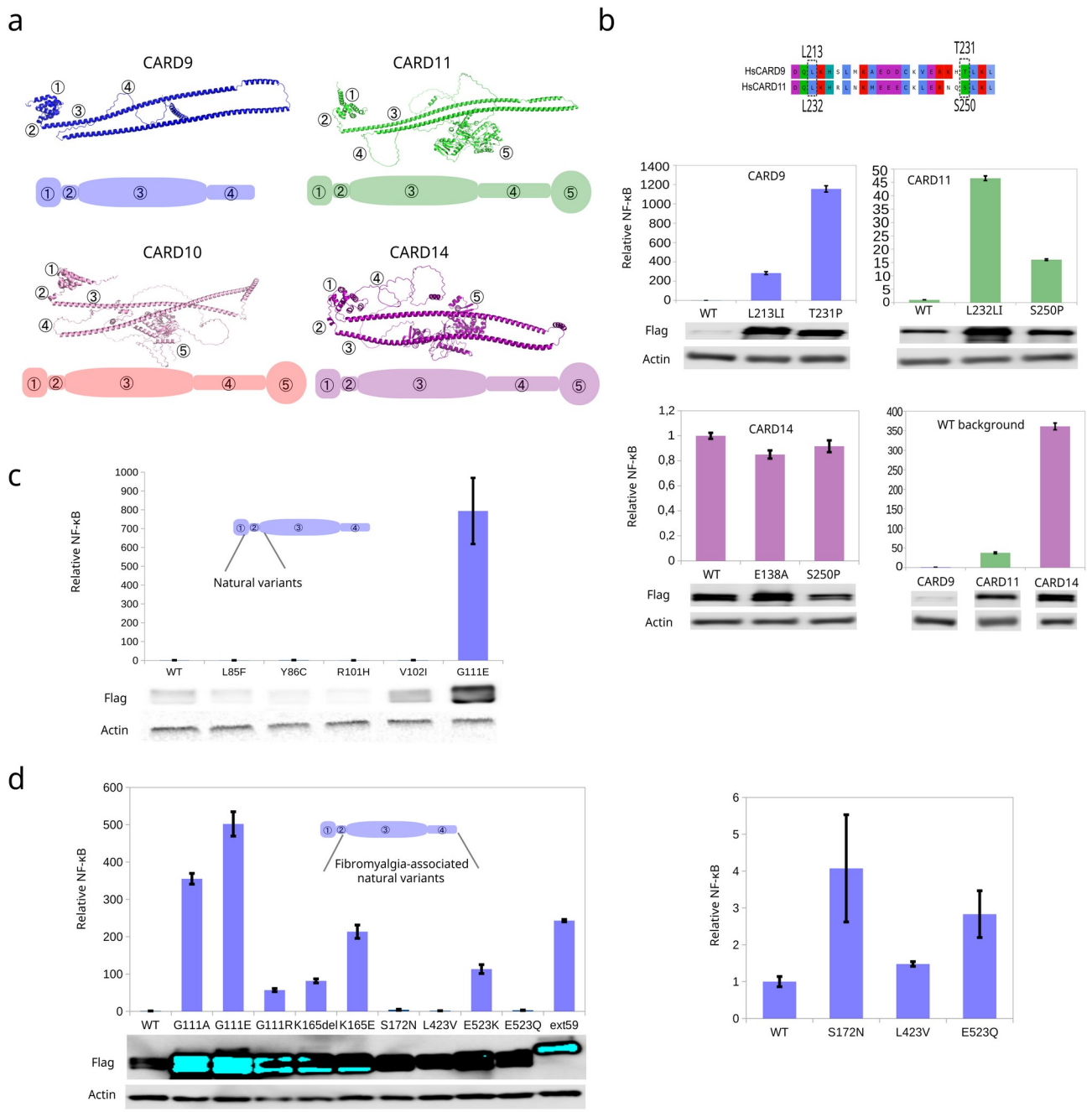

Figure 1

a) Comparison of the alphafold structures of the CARD-CC family members human CARD9 (structure Q9H257), mouse CARD10 (structure P58660), mouse CARD11 (structure Q8CIS0) and human CARD14 (structure Q9BXL6). Below: domain-composition cartoons with the colour codes used throughout the manuscript. The colour codes the same as the ones used for the phylogenetic analysis in [11]. Domains: ① = CARD, ② = LATCH, ③ = CC, ④ = Linker / ID, ⑤ = MAGUK.

b) NF-κB luciferase assay for transfered oncogenic CARD11 coil-coil mutations in CARD9 : L232LI ($CARD9^{L213LI}$) and S250P ($CARD9^{T231P}$). Relative induction compared to WT CARD9. Corresponding mutations in CARD11 ($CARD11^{L232LI}$, $CARD11^{S250P}$) relative to WT CARD11,

and CARD14^{S250P} and psoriasis-associated mutation CARD14^{E138A}, relative to WT CARD14. All done in a single experiment, but relevant relative comparisons presented sepparately for clarity.
c) NF-κB luciferase assay for potentially activating natural variant mutations in CARD9 at the CARD-LATCH-CC interface. Relative induction compared to WT CARD9.
d) Screening of natural variants of CARD9 associated to fibromyalgia in Genebass, and alternative substitutions at the same resisdues. Relative induction compared to WT CARD9. Weak activating mutations showed again on the graph to the right. Flag developed at high exposure to illustrate expression difference between WT CARD9 and the weak activating mutants.

All luciferase experiments have been repeated at least 3 times with similar relative trends. The error bars represent 1 standard deviation from 3-4 technical replicates (different transfections).

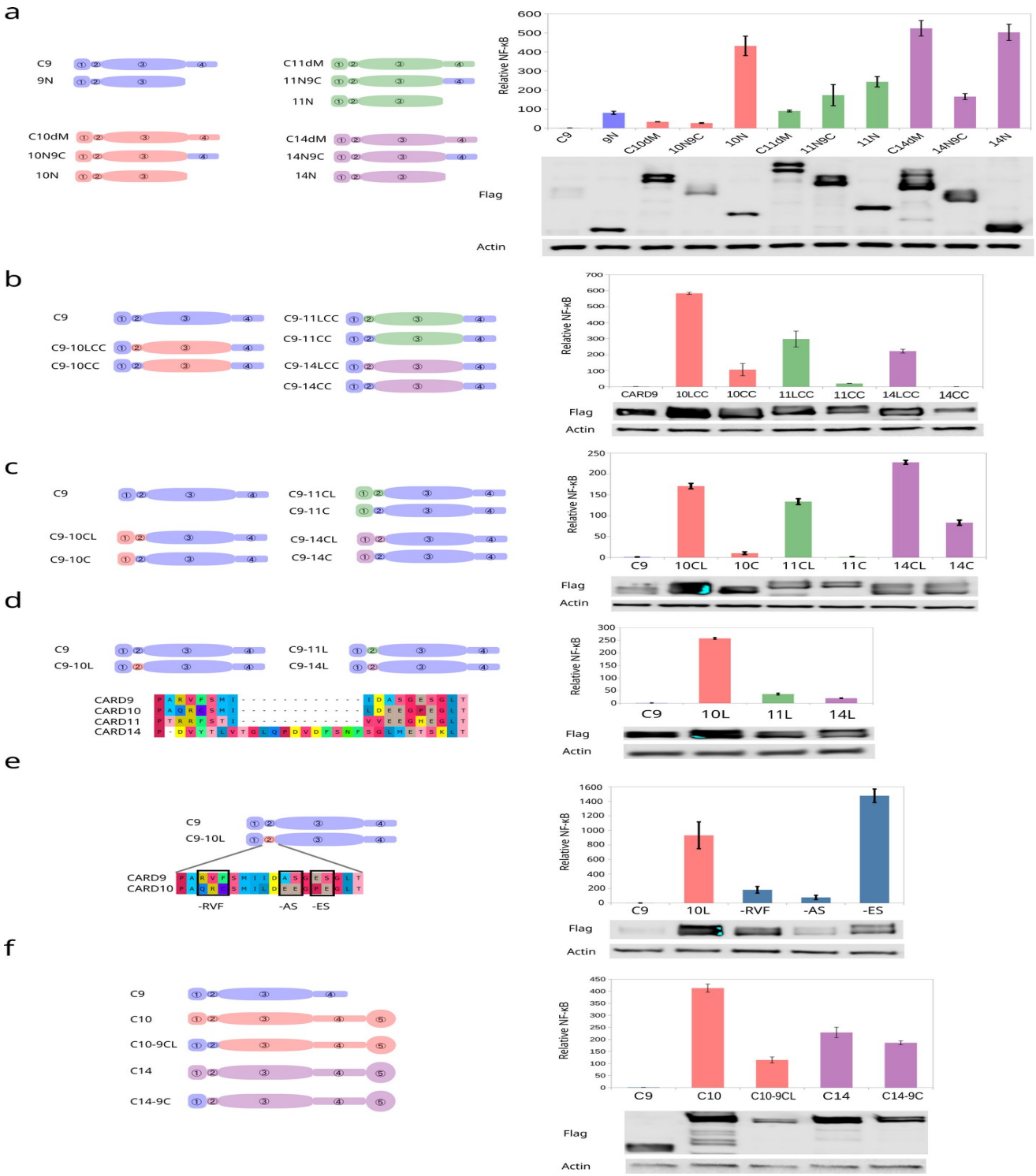

Figure 2

NF-κB dependent luciferase expression after overexpression of different Franken-CARD9 constructs. Relative induction compared to WT CARD9 (C9) and protein expression levels analyzed with anti-flag on a Western blot. All luciferase experiments have been repeated at least 3 times with similar relative trends. The error bars represent 1 standard deviation from 3-4 technical replicates (different transfections).

a) NF-κB luciferase assay for inhibitory activity of the CARD9 C-terminal sequence on CARD9, and the CARD-LATCH-CC fragments of CARD10, CARD11 and CARD14. Relative induction compared to WT CARD9.
b) Comparisons of CARD9 and CARD9 with the LATCH-CC or CC domain replaced with the sequence from CARD10, CARD11 or CARD14.
c) Comparisons of CARD9 and CARD9 with the CARD or CARD-LATCH domain replaced with the sequence from CARD10, CARD11 or CARD14.
d) Comparisons of CARD9 and CARD9 with the LATCH domain replaced with the sequence from CARD10, CARD11 or CARD14. Multiple sequence alignment of CARD9, -10, -11 and -14 LATCH domains.
e) Effects of specific substitutions between CARD9 and CARD10 LATCH domain on autoinhibition.
f) CARD9 CARD transplanted to CARD14 and CARD9 CARD-LATCH transplanted to CARD10 compared to the wild-type CARMA proteins.

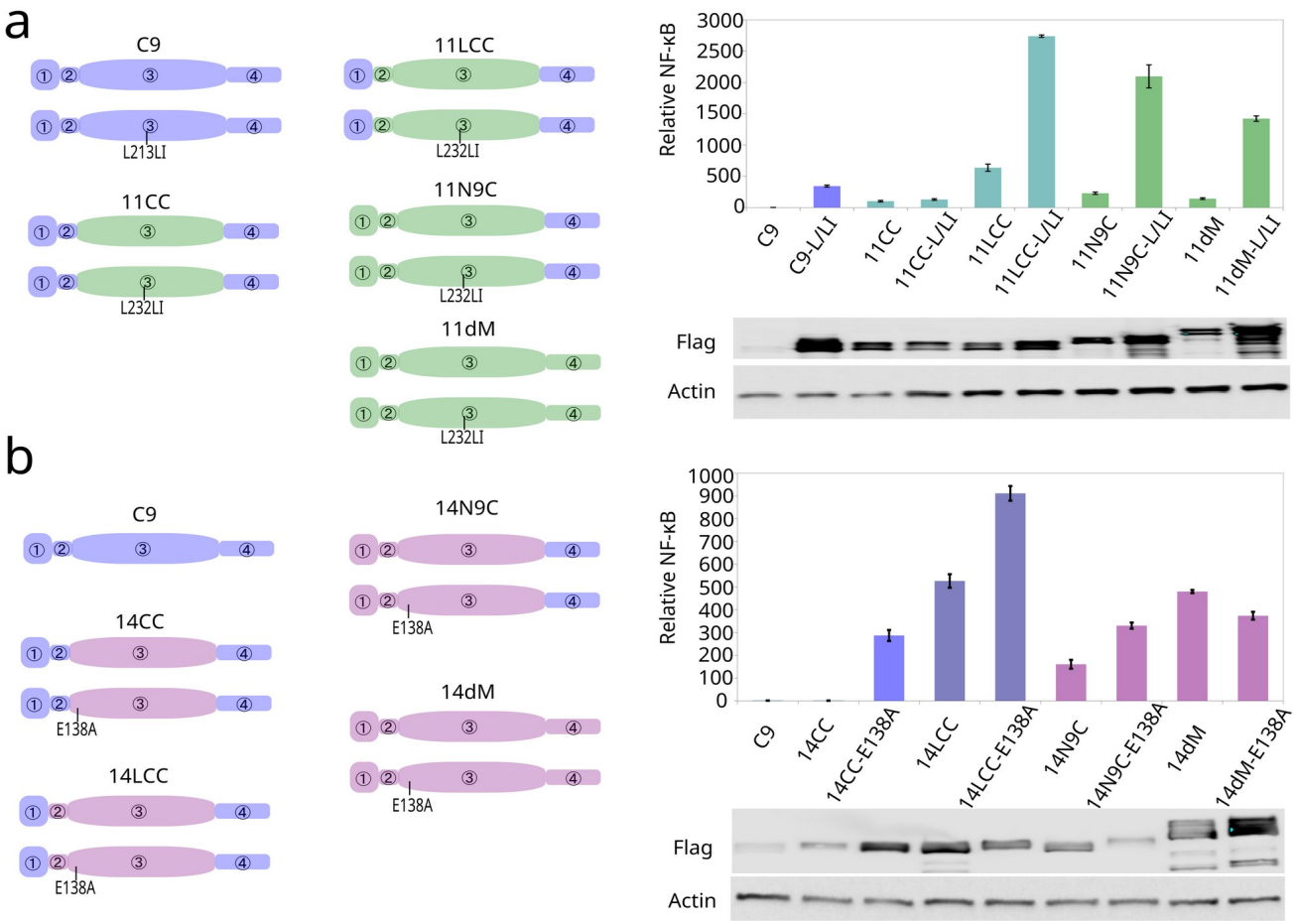

Figure 3

NF-κB dependent luciferase expression after overexpression of different Franken-CARD9 WT or activated mutant constructs. Relative induction compared to WT CARD9 (C9) and protein expression levels analyzed with anti-flag on a Western blot. All luciferase experiments have been repeated at least 3 times with similar relative trends. The error bars represent 1 standard deviation from 3-4 technical replicates (different transfections).

a) Comparison of the effect of the L232LI mutation in CARD11 in different Franken-CARD9 backbones, compared to WT and the L213LI mutation in CARD9

b) Effect of the CARD14 psoriasis-associated mutation E138A in different Franken-CARD9 backbones, compared to corresponding wild-type constructs.

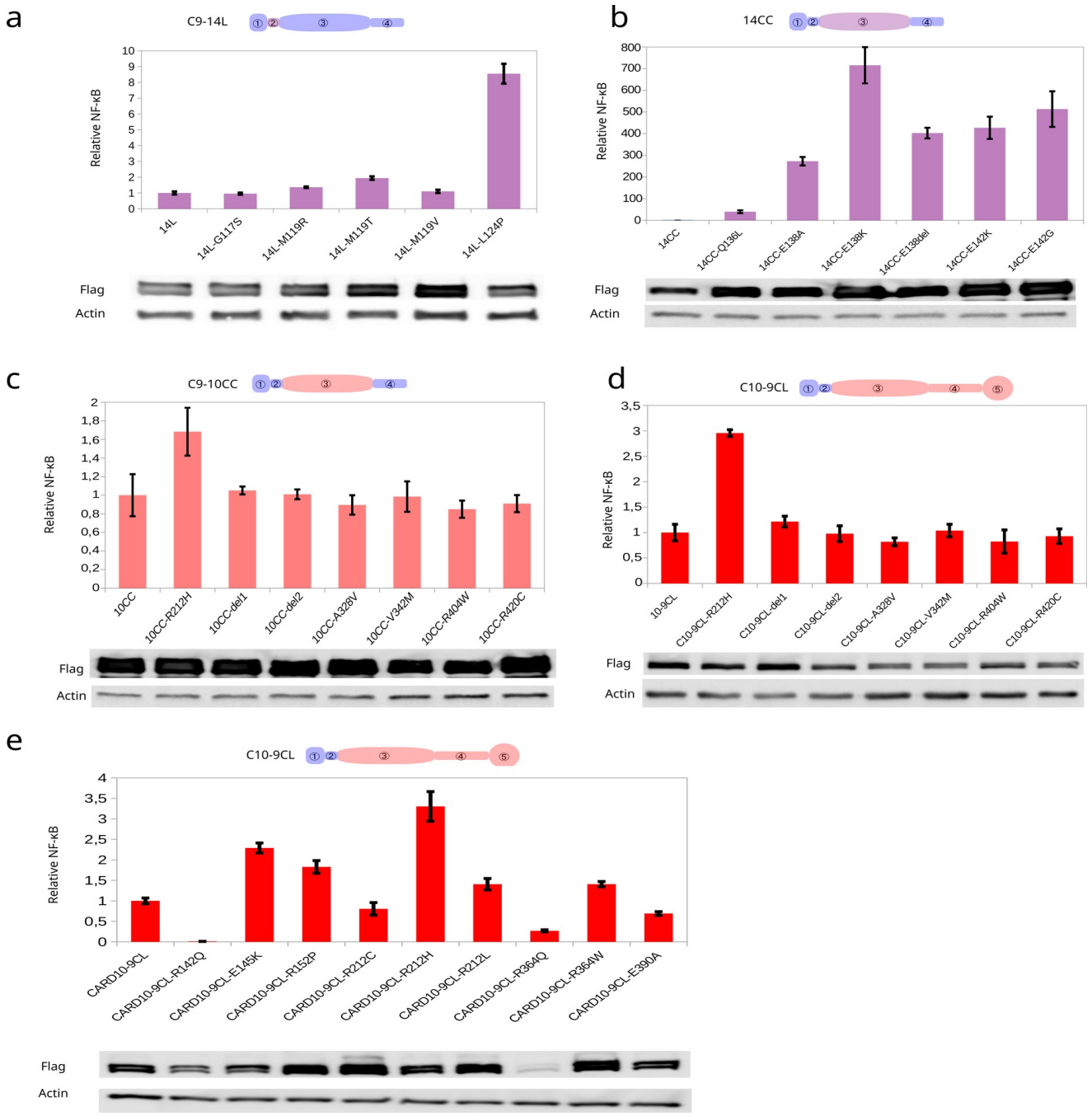

Figure 4

Proof-of-concept analysis of published mutations in the LATCH-CC region in CARD10 and CARD14, using the minimal Franken-CARD9 backbones with either the CARD9 LATCH or CC domain replaced with the corresponding sequence from CARD10 or CARD14. Only some mutations have previously been verified *in vitro* to be activating. Mutations are evaluated as relative NF-κB dependent luciferase expression after overexpression of different Franken-CARD9 constructs, compared to the the wild-type Franken-CARD9.

a) Evaluation of CARD14 LATCH mutations associated to psoriasis in the CARD9-14L

backbone.
b) Evaluation of CARD14 CC mutations associated to psoriasis in the CARD9-14CC backbone.
c) Evaluation of CARD10 CC mutations associated to POAG, cancer or autoimmune immunodeficiency in the CARD9-10CC backbone.
d) Evaluation of CARD10 CC mutations associated to POAG, cancer or autoimmune immunodeficiency in the CARD10-9CL backbone.
e) Evaluation of CARD10 natural variants with various Genebass disease associations overlapping with the associations found for R212H in the CARD10-9CL backbone.